AD_____

Award Number: W81XWH-05-1-0124

TITLE: Novel Protein Microarray Technology to Examine Men with Prostate Cancer

PRINCIPAL INVESTIGATOR: Hans Lilja, M.D., Ph.D.

CONTRACTING ORGANIZATION: Sloan-Kettering Institute
                           New York, NY 10021

REPORT DATE: December 2005

TYPE OF REPORT: Final

PREPARED FOR: U.S. Army Medical Research and Materiel Command
               Fort Detrick, Maryland 21702-5012

DISTRIBUTION STATEMENT: Approved for Public Release;
                        Distribution Unlimited

The views, opinions and/or findings contained in this report are those of the author(s) and should not be construed as an official Department of the Army position, policy or decision unless so designated by other documentation.

REPORT DOCUMENTATION PAGE

Form Approved
OMB No. 0704-0188

Public reporting burden for this collection of information is estimated to average 1 hour per response, including the time for reviewing instructions, searching existing data sources, gathering and maintaining the data needed, and completing and reviewing this collection of information. Send comments regarding this burden estimate or any other aspect of this collection of information, including suggestions for reducing this burden to Department of Defense, Washington Headquarters Services, Directorate for Information Operations and Reports (0704-0188), 1215 Jefferson Davis Highway, Suite 1204, Arlington, VA 22202-4302. Respondents should be aware that notwithstanding any other provision of law, no person shall be subject to any penalty for failing to comply with a collection of information if it does not display a currently valid OMB control number. **PLEASE DO NOT RETURN YOUR FORM TO THE ABOVE ADDRESS.**

1. REPORT DATE (DD-MM-YYYY)	2. REPORT TYPE	3. DATES COVERED (From - To)
01-12-2005	Final	22 Nov 2004 – 21 Nov 2005

4. TITLE AND SUBTITLE
Novel Protein Microarray Technology to Examine Men with Prostate Cancer

5a. CONTRACT NUMBER

5b. GRANT NUMBER
W81XWH-05-1-0124

5c. PROGRAM ELEMENT NUMBER

6. AUTHOR(S)
Hans Lilja, M.D., Ph.D.

E-mail: liljah@mskcc.org

5d. PROJECT NUMBER

5e. TASK NUMBER

5f. WORK UNIT NUMBER

7. PERFORMING ORGANIZATION NAME(S) AND ADDRESS(ES)

Sloan-Kettering Institute
New York, NY 10021

8. PERFORMING ORGANIZATION REPORT NUMBER

9. SPONSORING / MONITORING AGENCY NAME(S) AND ADDRESS(ES)
U.S. Army Medical Research and Materiel Command
Fort Detrick, Maryland 21702-5012

10. SPONSOR/MONITOR'S ACRONYM(S)

11. SPONSOR/MONITOR'S REPORT NUMBER(S)

12. DISTRIBUTION / AVAILABILITY STATEMENT
Approved for Public Release; Distribution Unlimited

13. SUPPLEMENTARY NOTES

14. ABSTRACT
We developed a novel macro and nanoporous silicon surface for protein microarrays to facilitate high-throughput biomarker discovery, and high-density protein-chip array analyses of complex biological samples. This surface offers 3D-surface enlarging properties and spot confinement, enabling both highly sensitive assays and high-density arrays with low imprecision. Relative standard deviation (RSD) of signal intensity both within and between chips were less than 20%. The detection limit and dynamic range of the novel protein chip surface was assessed with monoclonal anti-PSA IgG. Lower limit of detection was ≈0.7 ng/mL (26 pM) with linear detection (dynamic range) up to 104-fold higher levels.

We also developed microfluid-nanovial arrays to enable rapid proteolytic digestion linked to matrix-assisted laser desorption/ionization time-of-flight (MALDI-TOF) mass spectrometry. It uses minute amounts of sample and enhances both speed and accuracy in clinical applications of proteomics techniques, Automated picoliter microdispensing allows precise fluid handling in the microarray format. To assess this platform in a putative clinical application, two prostate cancer biomarkers, PSA and human kallikrein 2 (hK2) were digested at levels of 100 fmol (PSA), 20 fmol (PSA) and 8 fmol (hK2). All biomarker digestions were completed in less than 30 seconds, with successful MS-identification in the porous nanovial setting.

15. SUBJECT TERMS
Prostate Cancer, Biomarkers, Risk Assessment

16. SECURITY CLASSIFICATION OF:			17. LIMITATION OF ABSTRACT	18. NUMBER OF PAGES	19a. NAME OF RESPONSIBLE PERSON USAMRMC
a. REPORT U	b. ABSTRACT U	c. THIS PAGE U	UU	69	19b. TELEPHONE NUMBER (include area code)

Standard Form 298 (Rev. 8-98)
Prescribed by ANSI Std. Z39.18

Table of Contents

Introduction

Age-adjusted incident rates of prostate cancer slowly increase annually. This year, it is estimated that 234,460 men will be newly diagnosed with prostate cancer, and that 27,350 deaths will be caused by prostate cancer in US. As many more men die *with* rather than *of* their cancer (a ratio of about nine newly diagnosed cases for every one death), it is important to measure the threat to quantity and quality of life imposed by the disease. Major controversy exists whether the benefits outweigh the disadvantages of prostate-specific antigen (PSA) based early detection of prostate cancer, but a far greater prevalence of histological than life-threatening cancers may be used to support conservative, nonintervention-based approaches to disease. However, sufficient reliable diagnostic tools are currently lacking to accurately predict disease-risk prior to treatment.

Measurements of prostate specific antigen (PSA) levels in serum combined with digital rectal examination (DRE) have long been recommended as part of an early detection program for prostate cancer (1, 2). Nevertheless, the routine use of PSA as a screening tool is questioned due to lack of specificity when serum concentrations are moderately elevated as 70-75 % of men with PSA-levels from 4 to 10 ng/ml have negative biopsies. Identification and validation of biomarkers other than PSA are urgently needed to more appropriately select men for biopsy.

This proposal was designed to develop and validate novel, highly sensitive and specific means to identify and characterize a limited set of low abundance protein biomarkers for prostate cancer in blood samples. Together with routinely measured clinical and tissue characteristics – following appropriate validation in prospective clinical studies, these biomarkers could result in enhanced predictive models that will optimize patient treatment based on individual risk. In this project, we developed a novel porous silicon-based antibody microarray platform. The performance characteristics of the novel porous silicon-based antibody-arrays were characterized using serum or plasma from healthy female volunteers to which biotinylated proPSA was added *ex vivo*, and finally detected with FITC-labeled monoclonal anti-PSA IgG in a confocal microscope. The versatility of the novel porous silicon nanovials was explored using MALDI-TOF MS identification of signature peptides resulting from rapid tryptic digestion of a low abundant target protein (e.g. PSA or hK2). This novel technology will enhance our ability to search for new low abundant prostate cancer biomarkers in blood using a wide range of antibodies against various candidate biomarkers. We also assessed the utility of novel, highly sensitive and specific time-resolved fluorescence immunoassays to detect urokinase-type plasminogen activator receptor (suPAR) forms in blood to enhance discrimination of men with biopsy proven prostate cancer from men with no evidence of prostate cancer on biopsy. We used suPAR data in a prediction model, which also included PSA forms, which may importantly enhance discrimination of men with biopsy proven prostate cancer from men with no evidence of prostate cancer on the biopsy.

Body

Dr. Hans Lilja served as the Principal Investigator in this project. Involved in this project at Memorial Sloan-Kettering Cancer Center was also Dr. James Eastham, who served as a clinical investigator, Dr. Thomas Steuber, who served as a research fellow, and Todd Hricik, who served as the primary Research Technician. Dr. Thomas Laurell served as an important collaborator at Lund University, Sweden in the technical (particularly material-science based) development of the novel porous silicon-based antibody micro-arrays, while Kerstin Järås served as a research fellow at Lund University. Dr. Keld Danø served as an important collaborator at Copenhagen University, Denmark to provide access to reagents for the time-resolved fluorescent immunoassays of suPAR-forms in blood.

We developed a novel, high-throughput macro-/nano-porous silicon-based high density and high throughput antibody microarray platform. The performance characteristics of our novel, porous, silicon based antibody arrays (coated with monoclonal anti-PSA IgG) were characterized using serum or plasma from healthy female volunteers to which we added biotinylated proPSA *ex vivo*. Specific detection of the antigen-signal (after a wash step) was obtained using fluorescent detection of FITC-labeled streptavidin in a confocal microscope. We assessed the low end detection limit of the novel, high-throughput macro-/nanoporous silicon based high-density microarrays, which was shown to be about 0.7 ng/mL of PSA in serum (corresponding to about 25-30 picomoles of target antigen per liter). This assay manifested a highly extended dynamic range with linear signal detection obtained up to about 10^4 fold higher levels. Overall, we conclude that the performance characteristics of our novel fluorescent antibody microarrays for high density and high throughput search for novel candidate biomarkers correspond closely to those used for routine PSA measurements in blood.

The unique performance characteristics and versatility of the novel porous silicon array platform technology were further explored to assess dual-mode readout capabilities of the porous silicon microarray nanovials. Rapid peptide digestion of a target protein was completed followed by identification of signature peptides obtained from the digested target antigen using MALDI-TOF MS (Matrix Assisted Laser Desorption Ionization Time-Of-Flight Mass Spectrometry). We assessed the low end detection limits of MALDI-TOF MS identification of signature peptides resulting from optimized rapid tryptic digestion protocols of very small amounts of highly relevant low abundant prostate cancer targeted biomarker proteins (PSA and hK2). We first optimized the tryptic digestion protocols for the purified recombinant target proteins and found that we could dramatically decrease digestion times. Optimization of these protocols showed that we obtained complete digestion with trypsin in only 30 seconds. Secondly, we assessed our ability to identify critical signature peptides that would allow us to discriminate hK2 from PSA (which have ≈80% identity in primary structure) using high to low femtomole amounts of the target protein. These experiments showed that we could identify a critical signature peptide profile using 8 femtomoles of hK2, while the critical peptide signature readout obtained by MALDI-TOF MS discriminated the selected target protein (hK2) from PSA.

Finally, we assessed the utility of very recently developed, highly sensitive and specific time-resolved fluorescence immunoassays to detect suPAR forms in blood as a means to enhance detection and discrimination of men with biopsy proven prostate cancer from men with no evidence of prostate cancer on the biopsy. Three different assays provide the capacity to measure: circulating/soluble intact uPAR [uPAR(I-III)], intact uPAR + cleaved uPAR domains II+III [uPAR(I-III) + uPAR(II-III)], and cleaved uPAR domain I [uPAR(I)] with functional detection limits (total assay CV <20%) of 0.3 to 1.9 pmol/l. The detection limits are biologically relevant as they allowed us to measure detectable levels of each suPAR form in serum in all samples (referring to uPAR(I-III) and uPAR(II-III)), and in 384/390 patients sample (referring to uPAR(I)). Adding serum levels of both suPAR(II-III) and suPAR(I) to %fPSA and the conventional tPSA-levels enhanced AUC importantly (from 0.65 to 0.78; $p<0.001$). These findings were derived from a referral study cohort of 390 men, who were recommended according to current conventional practice to undergo systematic prostate biopsy. Histopathologic examination of samples from these patients revealed evidence of prostate cancer (n=224) or no evidence of prostate cancer (n=166). Finally, we used a multivariate logistic regression analysis to predict prostate biopsy outcome, where we included measurements of tPSA, %fPSA, suPAR(II-III), and suPAR(I), and found that each of these diagnostic tests contributed significantly ($p<0.05$) to enhance discrimination of men with biopsy proven prostate cancer from those with no evidence of prostate cancer on the biopsy – both across the entire study cohort, as well as for the men with only moderate PSA elevation in serum (2-10 ng/ml).

Key Research Accomplishments

Three stages of the outlined research have been completed, as follows:

1. We developed a novel, macro-/nano-porous, silicon based antibody microarray platform to enable high density and high throughput search for novel prostate cancer biomarkers in complex body fluids (e.g. blood) using fluorescent detection of FITC-labeled streptavidin. Performance characteristics assessed in a biologically relevant model system, using various amounts of proPSA added *ex vivo* to normal serum or plasma, showed a lower limit of detection in serum of ≈0.7 ng/mL (*i.e.* 25-30 pmol/l of target antigen), and a wide dynamic range with linear signal detection up to 10^4 fold higher. The results were published 2005 by Ressine et al (Appendix A).

2. The versatility of our novel, porous, silicon microarrays was further explored in efforts to enhance peptide digestion and MALDI-TOF MS based identification of signature peptides using a very small amount of a biologically relevant target protein biomarker for prostate cancer. We used purified recombinant PSA and hK2 (which share 80% identity in primary structure) to show that we may identify signature peptides (*i.e.* distinguishing hK2 from PSA) generated by a rapid (30 second) tryptic digest using less than 10 femtomoles of the target protein. The results were published this year by Finnskog et al (Appendix B).

3. We evaluated putative clinical utility of recent, highly sensitive and specific assays for various suPAR-forms [uPAR(I-III), uPAR(II-III), and uPAR(I)] to enhance prediction of prostate biopsies in men with moderate PSA elevation in blood. The detection limits of these assays (0.3 – 1.9 pmol/l) were sufficient to allow the planned clinical assessments, and we found that measurement of both suPAR(II-III) and suPAR(I) provided significant enhancements ($p<0.05$) in multivariate logistic regression analyses. AUCs were significantly greater when suPAR(II-III) and suPAR(I) were added to %fPSA and tPSA compared to tPSA alone (AUCs increase from 0.65 to 0.78; $p<0.001$) in a study cohort of 390 men who underwent systematic prostate biopsy. This showed that 224 men had prostate cancer, while 166 men had no evidence of prostate cancer (n=166). We also confirmed that these diagnostic enhancements remained for a subset of these men (n=255) who displayed only moderate PSA elevation in serum (2-10 ng/ml). These results were published this year in *Clinical Chemistry* (Appendix C).

All samples, purified biomarker forms, and antibodies were supplied by Drs. Hans Lilja, James Eastham, and Thomas Steuber at Memorial Sloan-Kettering Cancer Center. Study design and methodology were collaboratively determined by Drs. Lilja, Eastham, Laurell, and Danø.

With regard to the SOW stated for this award, we have addressed and delivered work tasks referring to Tasks #1 a-d, and #2a as described in the outlined stages above. We have not yet been able to assess the capability of our novel technologies to deliver the objectives delineated in task #2b-c. These tasks are currently being addressed, as are the objectives stated in work tasks #3 a-c. However, we have completed and submitted a

manuscript to *Clinical Chemistry* where we report on the use of various kallikrein form measurements in pretreatment samples in order to predict poor outcome in individuals diagnosed with prostate cancer as outlined in work task #3c (Appendix D).

Reportable Outcomes

Three publications have resulted directly from the work completed under this grant, and are included in the appendix:

A. Ressine A, Finnskog D, Malm J, Becker C, Lilja H, Marko Varga G, Laurell T. Macro/Nano-Structured Silicon as Solid Support for Antibody Arrays: Surface Design, Reproducibility, and Assay Characteristics Enabling Discovery of Kallikrein Gene Products for Prostate Disease Diagnostics. Nanobiotechnology;1(1):93-104. 2005.

B. Finnskog, D., Järås, K., Ressine, A., Malm, J., Marko-Varga, G., Lilja, H., Laurell, T. High-speed biomarker identification utilizing porous silicon nanovial arrays and MALDI-TOF mass spectrometry. Electrophoresis 27:1093-1103. 2006.

C. Piironen, T., Haese, A., Huland, H., Steuber, T., Christensen, I.J., Brünner, N., Danø, K., Høyer-Hansen, G., Lilja, H. Enhanced discrimination of benign from malignant prostatic disease by selective measurements of cleaved forms of urokinase receptor in serum. Clin. Chem. 52: 838-844. 2006.

The following manuscript is pending publication:

D. Steuber, T., Vickers, A.J., Serio, A., Vaisanen, V., Haese, A., Pettersson, K., Eastham, J.A., Scardino, P.T., Huland, H., Lilja, H. Comparison of free and total forms of serum human kallikrein 2 and prostate-specific antigen for prediction of locally advanced and recurrent prostate cancer. *Pending Publication.*

Conclusions

We developed and validated assay performance (lower limit of detection and dynamic range) of highly novel porous silicon-based antibody microarrays. The reported data show that the described assay performance (using biologically relevant model samples) is consistent with requirements to enable search for novel prostate cancer biomarkers occurring at moderately low abundance levels in complex body fluids (e.g. blood).

Biologically relevant biomarker targets (PSA and hK2) were used to assess performance of porous, silicon based, nanovial arrays for target protein identification/characterization using MALDI-TOF MS after rapid tryptic digestion of the putative target. These arrays enabled identification of critical signature peptides obtained from rapid tryptic digests of less than 10 femtomoles of hK2 (or PSA), which allowed discrimination between these highly similar proteins.

The dual-readout capacity of the reported porous silicon-based micro-arrays using both fluorescence detection and MALDI-TOF MS based identification of moderately low abundant prostate cancer biomarkers is a significant advancement, enabling high throughput search and identification of novel, low abundance prostate cancer biomarkers in blood.

We identified that measurements of several suPAR-forms [uPAR(II-III), and uPAR(I)] in blood may enhance prediction of prostate biopsy outcome in men with moderate PSA elevation in blood. This may contribute significantly in our clinical ability to counsel men with moderate PSA elevation in blood, specifically regarding whether they should (or should not) be recommended to undergo systematic prostate biopsy. However, it is evident that we would first need to confirm whether we would be able to replicate comparable diagnostic enhancements using other, independently collected, large size study cohorts, before making any definitive conclusions on these matters.

References

1. Catalona WJ, Richie JP, Ahmann FR, et al. Comparison of digital rectal examination and serum prostate specific antigen in the early detection of prostate cancer: results of a multicenter clinical trial of 6,630 men. J Urol;151:1283-1290. 1994.

2. Catalona WJ, Smith DS, Ratliff TL, et al. Measurement of prostate specific-antigen in serum as a screening test for prostate cancer. N Engl J Med;324:1156-1161. 1991.

Appendices
(in order of appearance in this section)

A. Ressine A, Finnskog D, Malm J, Becker C, Lilja H, Marko Varga G, Laurell T. Macro/Nano-Structured Silicon as Solid Support for Antibody Arrays: Surface Design, Reproducibility, and Assay Characteristics Enabling Discovery of Kallikrein Gene Products for Prostate Disease Diagnostics. Nanobiotechnology;1(1):93-104. 2005.

B. Finnskog, D., Järås, K., Ressine, A., Malm, J., Marko-Varga, G., Lilja, H., Laurell,' T. High-speed biomarker identification utilizing porous silicon nanovial arrays and MALDI-TOF mass spectrometry. Electrophoresis 27:1093-1103. 2006.

C. Piironen, T., Haese, A., Huland, H., Steuber, T., Christensen, I.J., Brünner, N., Danø, K., Høyer-Hansen, G., Lilja, H. Enhanced discrimination of benign from malignant prostatic disease by selective measurements of cleaved forms of urokinase receptor in serum. Clin. Chem. 52: 838-844. 2006.

D. Steuber, T., Vickers, A.J., Serio, A., Vaisanen, V., Haese, A., Pettersson, K., Eastham, J.A., Scardino, P.T., Huland, H., Lilja, H. Comparison of free and total forms of serum human kallikrein 2 and prostate-specific antigen for prediction of locally advanced and recurrent prostate cancer. *Pending Publication.*

Original Article

Macro/Nano-Structured Silicon as Solid Support for Antibody Arrays

Surface Design, Reproducibility, and Assay Characteristics Enabling Discovery of Kallikrein Gene Products for Prostate Disease Diagnostics

A. Ressine,[1] D. Finnskog,[1] J. Malm,[2] C. Becker,[2] H. Lilja,[2,3] G. Marko Varga,[4] and T. Laurell[1]

[1]Department of Electrical Measurements, Lund Institute of Technology, Box 118, 221 00 Lund, Sweden;
[2]Department of Laboratory Medicine, Division of Clinical Chemistry, Lund University, Malmö University Hospital, Malmö, Sweden; [3]Departments of Clinical Laboratories, Urology, and Medicine, Memorial Sloan-Kettering Cancer Center, New York, NY, USA; [4]Department of Analytical Chemistry, Lund University, Box 124, SE-221 00 Lund, Sweden

Abstract

To facilitate high-throughput biomarker discovery and high-density protein-chip array analyses of complex biological samples, a novel macro- and nanoporous silicon surface for protein microarrays was developed. The surface offers three-dimensional surface enlarging properties and spot confinement, enabling both high sensitivity bioassays and design of high density arrays. Reproducible manufacturing of the protein chip surface was accomplished as demonstrated by the low imprecision when standard IgG bioassays were performed at 100 pM antigen level on a series of protein chips scanned at widely different locations within a silicon wafer, as well as between different wafers from two different manufacturers. The relative standard deviation (RSD) of fluorescence spot intensity within an array on a chip was less than 20%. Mean spot intensity RSD was 19% for all 25 microarray chips in the study. Within-manufacturer-lot RSDs in chips from either manufacturer were <15% of mean spot intensity. The detection limit and dynamic range of the novel protein chip surface were examined to evaluate whether they match criteria required in a search for novel biomarkers such as for prostate cancer. Monoclonal IgG against prostate-specific antigen (PSA) was arrayed on the porous silicon chips. These were subsequently incubated in serum samples containing widely different levels of fluorescence-labeled PSA. Detection of PSA in serum at concentrations from 0.7 ng/mL (26 pM) up to 10^4-fold higher levels verified assay characteristics required in the search for prostate biomarkers (e.g., kallikrein gene products) at clinically relevant levels.

(Nanobiotechnology   DOI: 10.1385/Nano:1:1:93)

Key Words: Protein microarray; macro/nano-structured silicon; biomarker discovery; antibody.

Correspondence and reprint requests to:

A. Ressine,
Department of Electrical
Measurements, Lund Institute
of Technology, Box 118, 221 00
Lund, Sweden
E-mail:
Anton.Ressine@elmat.lth.se

Humana Press

Introduction

After completion of the human genome sequence project considerable efforts have been directed to the field of proteomics, analyzing the complete set of expressed proteins and their dynamic changes under biological perturbations such as disease development and progress or no progress during the influence of drug treatment (*1–5*). This task is haunted by the extreme complex nature of proteins, the high number of possible post-translational modifications, and their vastly diverse chemical characteristics. Microarray technology, invented less than a decade ago, already has greatly impacted genomic research and is currently seen as a highly potent complementary technology platform for proteome mapping (*6–8*).

Array-based profiling techniques are conceptually simple. A protein microarray

device is a chip that contains a collection of miniaturized test sites, e.g., spots. A molecular affinity probe, specific for a particular analyte, is immobilized at a defined test position in a two-dimensional array, each position holding a different probe. The interaction of the probe molecules, i.e., antibodies, with their target molecules is subsequently detected by optical, electrochemical, mass spectrometric, radioactive, or other analytical readout *(9)*. Signals form each probe site indicate that interactions have occurred, their intensity and position in the array are recorded, and thus the target molecules and optimally also their quantity can be identified.

As an emerging field protein microarray technology still presents many essential challenges that should be addressed. These challenges can be classified in relation to the following categories: what probes are immobilized (the choice of affinity probe), onto what are they immobilized (the choice of surface/immobilization matrix), and how are they immobilized (probe immobilization method) *(10)*.

A high specificity to the target analyte is a fundamental requirement for the probe molecules. Because the ideal microarray should have thousands or may be even more specific sites on a single chip, the absence of cross-reactivity is a stringent requirement for the probes. Antibodies are commonly used as affinity probes to fulfill these requirements as far as possible. The immobilization method is also very important, as it greatly affects the ability of the probe to bind the analyte. Physical adsorption and chemical cross-linking (oriented or random) are the most frequently used methods of choice for immobilization. Last, but not least, a major challenge is the choice of surface for probe molecule anchoring. Parameters to take into account in this respect are:

- immobilization efficiency (the number of active probe molecules bound to the surface)
- ratio of the unspecific binding of analyte to the surface outside the test sites vs specific binding to the probe site
- probe binding kinetics

All of the above are also strongly affected by the surface type *(10,11)*. Thus, the choice of surface for immobilizing the probes is of the utmost importance and, with regards to the current technology level, a further advancement can be anticipated where not only surface material and chemistry *(12–16)* but also the micro- and nano-morphology *(17)* are considered for optimal chip performance. The following criteria are key factors necessary to consider in order to achieve a good matrix/substrate for protein microarray applications:

- low surface background intensity (e.g., when fluorescence readout is employed)
- mild immobilization conditions to prevent probe molecules from denaturation
- high immobilization efficiency

- low surface wetting, enabling high-density arraying
- uniform distribution of probe molecules over the test spot, enabling enhanced dynamic detection range and lower limit of detection

The commonly observed non-uniform probe distribution over a microarray test spot is known as the "coffee ring" effect. This is attributed to the micro advection mechanism in a drying droplet, enriching molecules in solution or material in suspension at the edge of the spot during the evaporation of the solvent *(18,19)*. This effect can to a great extent be avoided using true 3D structured surfaces.

Our group has developed an approach utilizing macro/nanostructured porous silicon surfaces as a 3D surface matrix for protein immobilization *(17,20)*. Porous silicon (PS) has a high surface to volume ratio, 200–800 m^2 cm^{-3}, and the porosity can vary mainly between 10% and 90% volume ratio *(21)*, offering properties of surface area enlargement that are beneficial in applications of biomacromolecule immobilization. Because the morphological properties of porous silicon can easily be altered by changing fabrication conditions, the material can be tuned to the specific requirements of a bioanalytical application *(22)*.

PS has been used mainly in optical applications, because of its excellent luminescence properties *(23)*, and as an electrical insulator material *(24)*, although recent work from our group utilized it in bioanalytical and proteomics applications *(25)*. For example, nano/- and macro-structured silicon has successfully been used in enzyme microreactors to gain immobilization efficiency *(26)*. The increased textured surface area allows the immobilization of more molecular species in the surface layer of a substrate as compared to a planar surface and thus obtaining an increased chemical activity.

A most striking fact is that it is also possible to achieve hydrophobic properties on PS surfaces with water contact angles up to 110° *(20)*. It was further shown that the low surface wetting property improves spot confinement and thus allows a higher spot density on the chip. Consistent with the theories proposed by Ekins and collegues *(27,28)*, reduction of the spot area during probe deposition also results in increased binding kinetics (formation of an antibody antigen complex) and readout sensitivity. Hence, proving the principle of "the smaller the probe spot size, the better." Another advantage of PS is that silicon structures can first be generated on bulk wafers with standard photolithography, which subsequently can be porosified *(29)*, enabling them to be included in microfluidic networks for bioanalysis of complex biological fluids.

Reproducible manufacturing of the support material is an inherently important issue in affinity-based separation and analytical applications *(30)*. As the PS fabrication process is dependent on a multitude of process parameters (crystal orientation, silicon dopant type, dopant level, current density, illumination, electrolyte composition, tem-

perature, and so on), the reproducibility of the fabrication process could be relatively unstable in a certain range of fabrication conditions. In this article the up-scaling and reproducibility of the micro/ nanoporous silicon fabrication process is investigated with respect to the bioanalytical readout as detected in antibody–antigen interactions (anti-IgG/IgG-FICT). The performance of the obtained protein chip surfaces was also demonstrated in a prostate-specific antigen (PSA) assay, showing a detection level of 26 pM (0.7 ng/mL).

Materials and Methods

Materials

Unless otherwise specified, all chemicals were purchased from Sigma-Aldrich GmbH (Schnelldorf, Germany). Dimethylformamide (DMF) was 99.8% chemical pure grade solution and hydrofluoric acid (HF) 40% solution was from Merck KGaA (Darmstadt, Germany). The antibody–antigen pair used in the reproducibility studies was goat anti-rabbit IgG and rabbit IgG from Sigma-Aldrich (St. Louis, MO, USA). For PSA studies the monoclonal IgG 2E9 raised again PSA was first described in *(31)* and was provided by Department of Laboratory Medicine, University Hospital, Malmö, Sweden.

Silicon wafers with different orientation and doping levels were obtained from Addison Engineering Inc. (San Jose, USA), Topsil Semiconductor Materials A/S (Frederikssund, Denmark), and Siltronix, SAS (Archamps, France).

Porous Silicon Fabrication

The fabrication set up and design of the liquid cell for electrochemical silicon etching is described in more detail elsewhere *(26)*. For this work we used a two-compartment electrochemical cell providing electrolyte contacts to the wafer from both sides and also having a transparent sapphire glass (Melles Griot BV, Netherlands) window on one side of the electrochemical cell to allow illumination during anodization if needed. The electrochemical cell was designed to work with 3 in. silicon wafers. The following process conditions were used for the porous silicon surface preparation:

- Morphology A was generated by anodization of *p*-type silicon wafers from Siltronix with (100) crystal orientation and resistivity of 20–70 $\Omega \cdot$cm without backside illumination. A current density of 8 mA/cm^2 was applied for 20 min. The electrolyte was a 1:3 mixture by volume of 40% HF and 95% ethanol.
- Morphology B was generated by anodization of *p*-type silicon wafers from Topsil Semiconductor Materials A/S with (100) crystal orientation and resistivity of 10–15 $\Omega \cdot$cm as well as Addison Engineering Inc. wafers with (100) orientation and 1–20 $\Omega \cdot$cm resistivity. The backsides (anodes) of the wafers were illuminated during the complete anodization period using a 100 W halogen lamp

(Osram, Germany) at a distance of 10 cm from the transparent window on the backside of the electrochemical cell. A current density of 2 mA/cm^2 was applied for 1 h. The electrolyte was a 1:10 mixture by volume of 40% HF and 99.8% DMF.
- Morphology C was generated by anodization of *p*-type silicon wafers from Topsil Semiconductor Materials A/S with (110) crystal orientation and resistivity of 20–70 $\Omega \cdot$cm. The backside of the wafer was illuminated during the complete anodization period at a distance of 2 cm from the window on the back side of the electrochemical cell. A current density of 10 mA/cm^2 was applied for 10 min. The electrolyte was a 1:1 mixture by volume of 4.5% HF and 95% ethanol.
- Morphology D was generated by anodization of silicon wafers from Addison Engineering Inc. with (100) orientation and 1–20 $\Omega \cdot$cm resistivity in a 1:10 mixture by volume of 40% HF and 99.8% DMF. A current density of 10 mA/cm^2 was applied for 40 min.

IgG Assay

The chips were mounted onto a plastic slide sized to fit the standard microscopic glass slide format (upper inset on Fig. 1). Anti-rabbit IgG (aRIgG) was spotted onto the chip surfaces with a piezoelectric dispenser, delivering approx 100 pL droplets per position. The antibody solution was 1 mg/mL concentration in PBS buffer (10 mM, pH 7.4) and only 5 μL of antibody solution was required to load the microdispenser. The spot-to-spot distance was set to 100 μm, resulting in microarray densities of 10,000 spot/cm^2. The chips were subsequently washed three times in 10 mL of PBS containing 0.05% v/v Tween-20 (PBS-Tween) with agitation in a shaker (each washing 5 min) to remove loosely bound antibodies from the surface. Afterward the chip surface was blocked with 5 wt% non-fat milk in PBS for 20 min to passivate the surface outside the spotted areas followed by washing. Finally, microarrays were incubated with 30 μL of human plasma solutions spiked with RIgG-FITC for 1 h followed by a final extensive washing step. The fluorescence read-out was performed with a confocal microscope FluoView 500 (Olympus, Japan), with an excitation wavelength of 488 nm. An oil immersion 20x objective was used.

PSA Assay

The monoclonal capture antibodies raised against PSA were spotted onto the chips in the same way as described for anti-RIgG above. The antibody solution concentration was 500 μg/mL in PBS. The spot-to-spot distance was set to 100 μm. After arraying, the chips were washed three times in 10 mL of PBS-Tween with agitation in a shaker (each wash lasted 5 min). Subsequently, chips were blocked with 5 wt% non-fat milk in PBS for 20 min. Finally, microarrays were incubated for 3 h with human serum spiked with PSA-FITC to the different concentration levels specified followed by a final
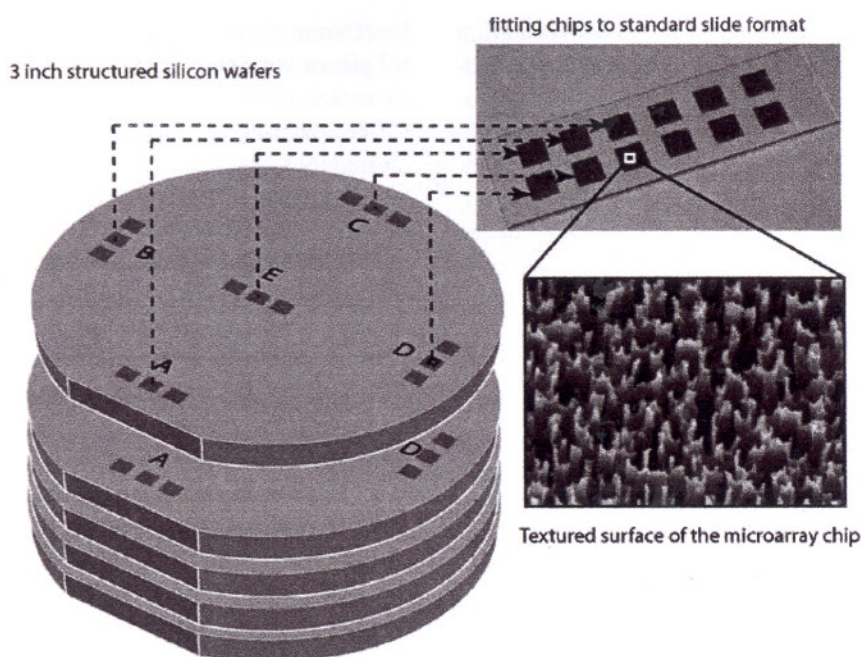
Fig. 1. Wafer scale processing for the fabrication of macro/nanostructured silicon microarray chips from 3-in. silicon wafers. A,B,C,D indicate the positions on the wafer from which chips were taken for the reproducibility study.

extensive washing step. Confocal fluorescence provided the readout.

Results and Discussion

Fabrication of Micro/Nanostructured Porous Silicon

We developed a process for scaling up the fabrication of macro/nanostructured PS microarray chips. Three inch wafers were porosified by electrochemical dissolution in a HF solution. The porosified wafers were diced into 6×6 mm^2 dice, producing about 70 chips from a single wafer. The chips were further fitted on a standard microscopic glass slide format, as shown in Fig. 1, optionally allowing use of commercially available arraying stations and confocal scanners.

The simplicity of the PS processing contrasts with the great variety of porous morphologies (pore diameter, shape, orientation, branching, and density) that can be obtained. These are strongly dependent on several physical/chemical parameters, e.g., silicon crystal orientation, type and doping level, as well as the composition of the electrolyte solution (HF concentration, organic additives) and anodization parameters (time, current density, illumination conditions). This multidimensional process parameter space is the means to tailor the structure of the 3D matrix to specific applications. By tuning the 3D surface structure of a silicon chip, the wetting as well as the optical properties can be optimized.

Physical Properties of the Porous Silicon Substrate

Figure 2 represents several morphologies fabricated and tested for protein microarray applications in our lab. In this image we show that porosity, pore size, pore density, and geometrical factors of the pores can be controlled.

The generated macro/nanostructured PS layers were 3D matrices having a combined topology of macropores with a characteristic pore size in the micrometer range (0.5–1.5 μm) mixed with a nanoporous structure with pore sizes in the nanometer range. This combined pore morphology is seen in Fig. 2A, where a nanoporous network in the macropore walls is resolved in the inset image. The insets in Fig. 2 show the top views of the presented morphologies and illustrate the geometry/shape of the pore tips, from being more rounded on the C sample to become very sharp peaks on the B and D matrices and to a foam-like shape on the A-type matrix. The macropore density was tuned with the highest density observed for Sample B. It is clear that all these morphology factors affect the probe deposition drastically and thus will influence the final bioanalytical signal readout.

For fluorescence microarray applications, we selected morphology B, which showed the optimal wetting behavior and the most uniform fluorescent spot intensity. Furthermore, the macro/nanostructured silicon substrates developed showed absence of photoluminescence in the green and red range of the spectra, making them compatible with fluorescence readout measurements.
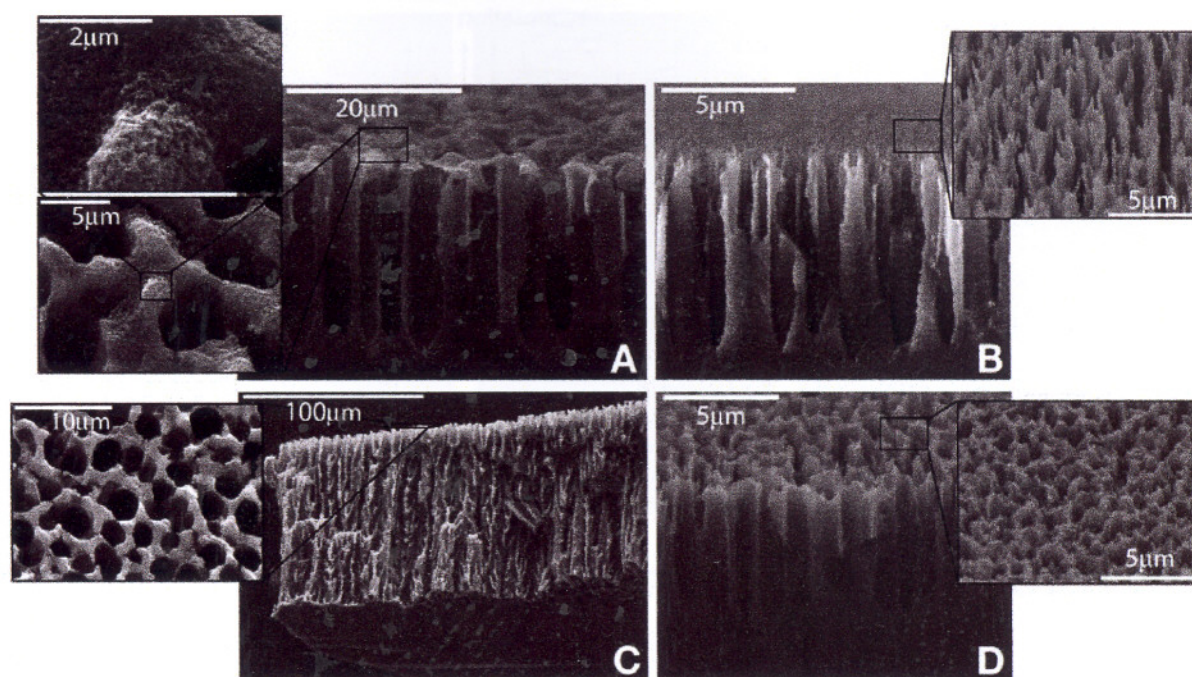
Fig. 2. Controlled preparation of the macro/nano PS matrices with different morphologies.

The choice of the porous structure shown in Fig. 2B for the protein chip applications was made as the result of our previous work *(17,20)*, also in accordance with the priority list for protein chips, given above.

Surface Wetting

There are several reasons why low surface wetting (i.e., high contact angles on the surface during drop deposition) is beneficial. First of all, high-density microarraying is inherently achievable. Reducing the spot size allows a decrease of the spot-to-spot distance without risk of cross-contamination between adjacent microarray spots. In this work we report on spot densities of 10,000 spots/cm² with a single spot diameter of about 50 μm and spot-to-spot center distance 100 μm as seen in Fig. 7. Another important factor is the increase of the probe density over the spot area. For example, the reduced spot size of a factor of 2 inherently led to a fourfold average increase in probe molecule density over a single dry spot. As also has been described by Ekins *(28)*—one of the pioneers in the microarray technology—the reduced spot size leads to increased binding kinetics of the bioassay performed.

Spot Homogeneity

Generally, the probe molecules are dissolved or suspended in a solvent of which a droplet is applied to a certain position on the surface along with new droplets containing other probe molecules, forming an array. The array is then dried to remove the solvent, leaving spots of affinity probes on the chip surface. The drying of a droplet commonly leaves a ring

on the surface with the reagent concentrated at the spot perimeter. This concentration gradient across the spot is highly undesirable, as it reduces the readability of the spots. It would therefore be advantageous to provide a spot with a probe concentration profile that is more uniform, holding the same probe density in the ring stain over the complete spot area. The physical mechanism lying behind the "coffee ring" effect is based on micro advection in the deposited droplet while drying and is well described in the literature *(18,19)*. Briefly, because the contact line of the droplet is pinned to the surface and the evaporation rate is higher at the edge of the spot, a net advective flow from the droplet center to the edges of the spot is induced (Fig. 3A). This radial micro flow balances the evaporation at the spot perimeter and, as the solute molecules are drawn to the edge, the solvent evaporates whereby the dissolved species are concentrated at this location until the spot is completely dry forming a ring pattern exactly as when a coffee spot is drying (Fig. 3B).

One way to avoid this is to break down or reduce the advective flow while the deposited droplet is drying. By increasing the contact angle to be larger than 90° for the deposited droplet volume, and having a smaller wetted spot area, the evaporation rate close to pinned line is actually lower than along the spherical fluid surface/air interface. Dissolved species are thereby not enriched at the spot perimeter. In the very late phase of droplet drying, where the contact angle is low (<90°), solute flow to the perimeter can take place to a certain extent. The end result of the low wetting (high contact angle) of the macro/nanoporous
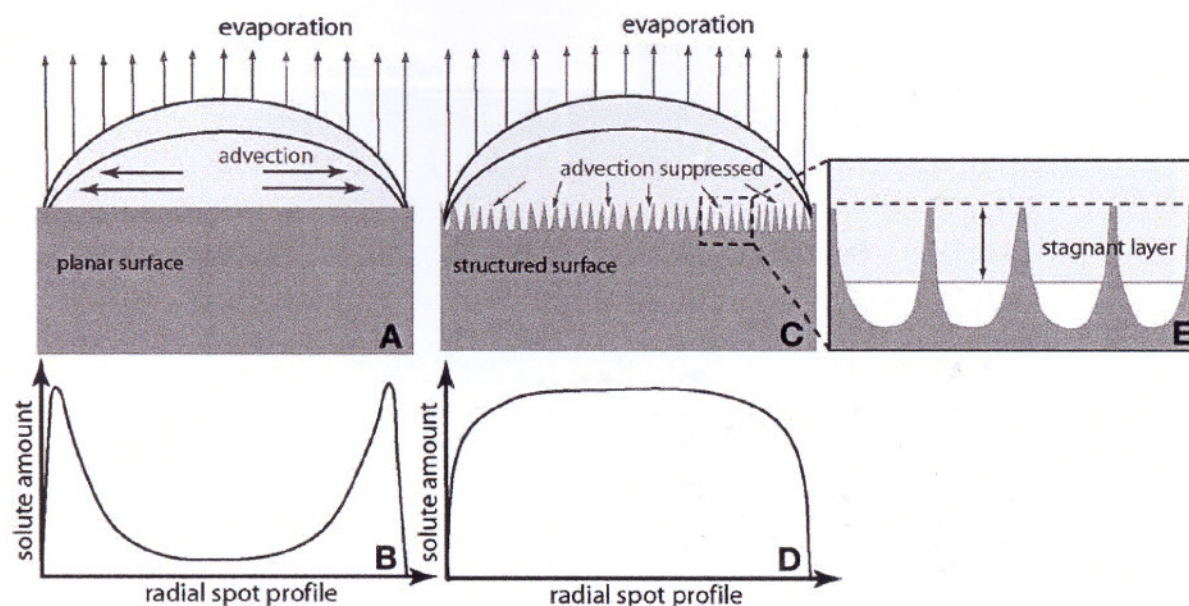
Fig. 3. The mechanism of ring formation during drop deposition on planar surfaces **(A)** the resulting probe distribution over a spot on planar surface **(B)**; **(C,E)** suppression of advection on textured surfaces, and **(D)** the corresponding spot distribution.

surface is that the enrichment of molecular species along the spot perimeter is substantially suppressed as compared to the case where the initial contact angle of the droplet volume is lower than 90°. We also find that on the obtained surface morphology liquid penetrates to some extent into the porous layer ($\approx 10 \ \mu$m), forming a stagnant fluid layer. During the final phase of droplet evaporation on the structured surface, the highly concentrated liquid surface layer penetrates into the porous layer, which displays a higher hydrodynamic flow resistance to the spot edge, suppressing evaporation-driven advective flow (Figs. 3C,E). This will further contribute to a more homogeneous spot coverage of a dissolved bioanalyte (Fig. 3D).

An important aspect in this reasoning is the fact that the solid surface onto which the probe molecule is immobilized actually is hydrophilic, although the morphology makes the surface act hydrophobically. The risk of hydrophobic denaturing of the biomolecule on the surface is thereby avoided, which otherwise would be the outcome if a conventional hydrophobic surface material was chosen to accomplish similar effects.

Figure 4 illustrates the relationship of the surface wetting and surface structure versus probe spot size and density of analyte immobilization. To emulate the probe distribution during deposition, we dispensed rabbit IgG (RIgG) conjugated with FITC (1 mg/mL solution in PBS) on three different surfaces: two planar surfaces (glass microscopic slide and aminosilanized glass) and one textured surface (macro/nanostructured silicon) (Fig. 2B). The antibody solution was spotted in 100 pL drops (one drop per position) and arrays were then washed. For microscopic glass slides and aminosilanized glass, water contact angles were 15° and 60°, respectively, the spot sizes of RIgG-FITC single spots were 200 and 120 μm in diameter correspondingly,

while for structured PS chips the average spot size was about 50 μm and water contact angles were about 110°. The immobilization efficiency of the labeled RIgG also increased when spot size decreased, as can be seen in the intensity of the fluorescent image (Fig. 4.). The coffee ring effect was observed on both planar surfaces, but not on the macro/nanostructured silicon substrate.

Reproducibility of the Macro/Nanoporous Surfaces

A fundamental requirement for the success of a new microarray surface is that the surface properties can be readily reproduced on chips in large numbers and long batch series. As PS is known to feature nonstable surfaces and sensitive process conditions, this material is commonly not considered optimal for the requirements set for a protein microarray chip surface. Even with commercially available supports, there are enormous differences from one manufacturer to another, not to mention lot-to-lot variations from the same manufacturer. Without doubt, manufacturing of reproducible supports is a major concern inherent with affinity-based separations and analysis, which successfully has been addressed and resolved by industry through strong requirements on process control.

To investigate the reproducibility of the developed PS fabrication protocol when scaling up to 3 in. wafer scale and comparing wafer to wafer, we performed the same IgG bioassay on the chips made from different positions on porosified 3-in. silicon wafers. The assay protocol is described in the Material and Methods section.

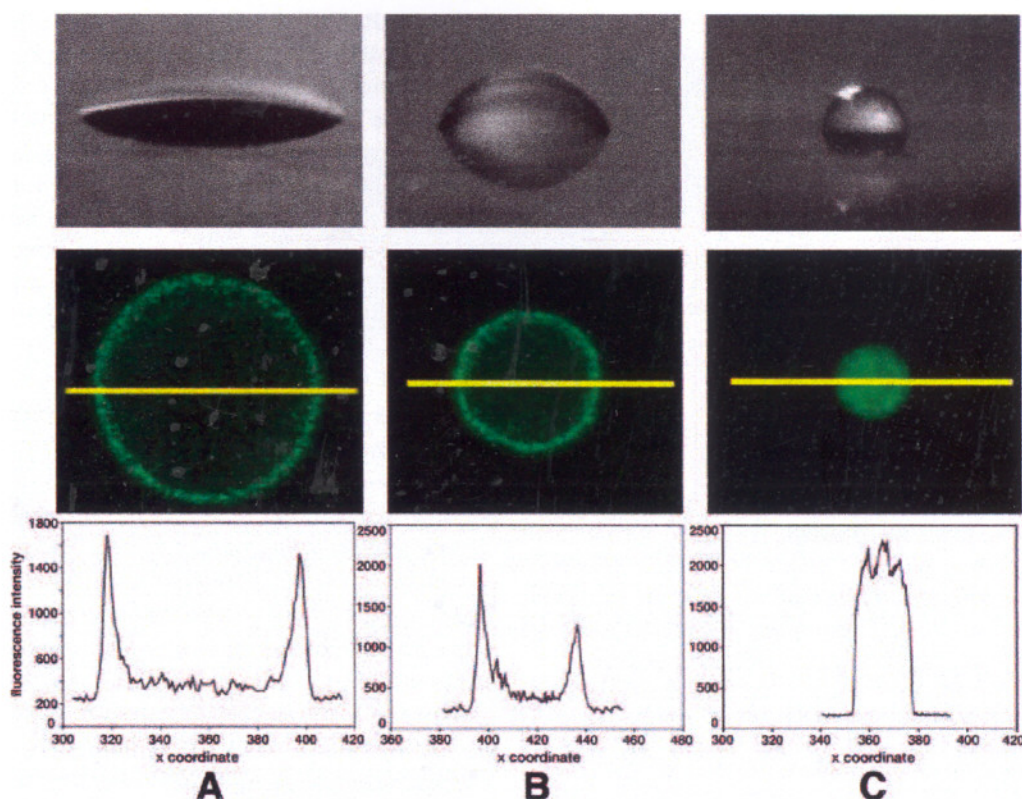To represent the whole surface, chips were taken from the positions denoted A,B,C,D, and E as shown in Fig. 1. The

Fig. 4. The contact angles during probe deposition/spotting (top) and probe molecules distribution shown as fluorescence intensity (middle) and fluorescence profile along the yellow lines on the three compared surfaces (lower): **(A)** microscopic glass slide, **(B)** aminosilanized glass, and **(C)** macro/nanostructured silicon chip. 100 pL droplets of RIgG-FITC solution in PBS were spotted. A "coffee ring" effect was observed on the microscopic glass slide and aminosilanized glass, while macro/nanostructured silicon showed a more homogeneous profile.
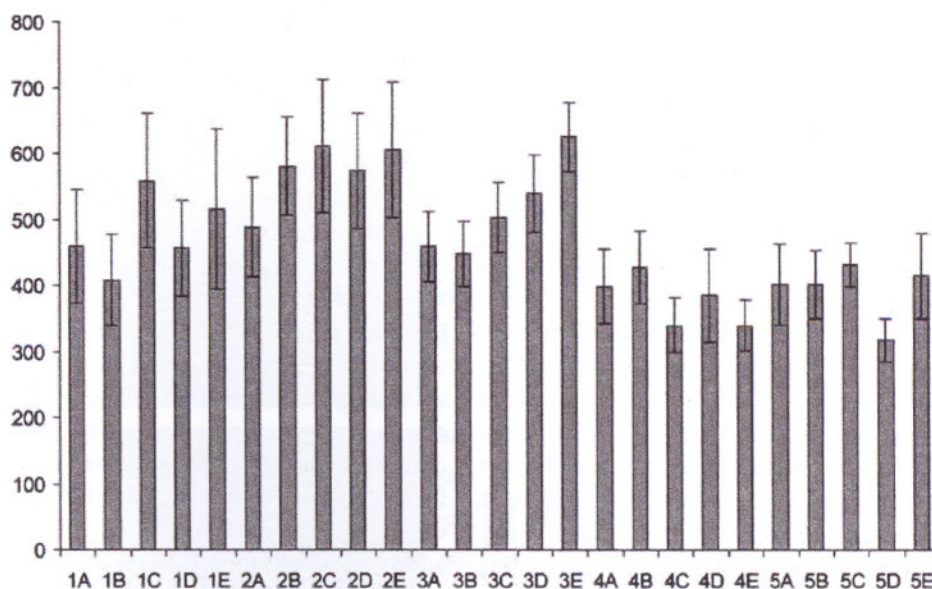

Fig. 5. Comparison of the mean spot intensity on the A,B,C,D,E chips and wafer-to-wafer (1–5) variations. Error bars indicate the standard deviation in fluorescent spot intensity for 30 spots within the corresponding chip (1A–5E).

same protocol was applied for all chips diced from their corresponding positions (A–E). The study aimed at revealing if major variations in bioassay response could be detected in relation to the individual spatial position of the chip (A–E) on the wafer and between different wafers (1–5) (Fig. 5). This in turn could possibly be traced back to variations in
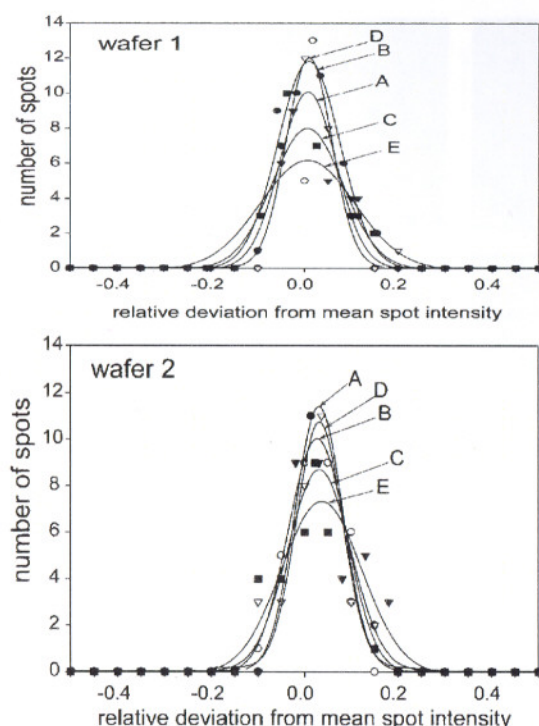
Fig. 6. Relative deviation of the single spot intensity from mean value for the chips A,B,C,D,E. The chips originated from two wafers made at different times. Microarrays with immobilized aRIgG were incubated in plasma spiked with 100 p*M* of RIgG-FITC . Thirty spots on each chip were analyzed.

surface morphology and variations in the electrochemical anodization process. However, there was good reproducibility for chips within the wafer as well as between different wafers. No differences between the chips were observed by visual inspection, which normally is a very good indicator for detecting morphology variations on porous silicon surfaces. Contributions to observed standard deviations may originate from the manual handling (washing and application of incubation solution, and so on), and non-perfect assaying conditions such as stagnant chip incubation (no agitation). It was observed that wafers 4 and 5 showed a lower level of overall bioassay performance, which may be explained by manufacture-to-manufacture variation, as wafers 4 and 5 were from different manufacturers and as these wafers actually deviated in the phosphorus dopant concentration. Wafers 1–3 were purchased from Topsil with a bulk silicon dopant concentration of 10–15 Ω·cm, and the wafers 4–5 were obtained from Addison, with a bulk silicon dopant concentration of 1–20 Ω·cm. It was concluded that the difference in resistivity also affected the porous morphology as seen in the slightly lower bioassay readout. The mean fluorescence intensity for all 25 chips in the reproducibility study was 467±89 [AU], i.e., an RSD of 19%. The corresponding RSD for only the Topsil and the Addison chips were, respectively, 13% and 10%.

As an alternative method to characterize the quality of the PS protein chip and the performed bioassay, the relative deviation to the mean spot intensity was estimated for each of the chips taken from two wafers (wafers 1 and 2) (Fig. 6).

The width of the relative deviation in mean spot intensity is indicative of the spot to spot reproducibility and is generally observed to be below ± 0.2. Other work on protein micro arrays report similar data also claiming a good spot to spot reproducibility (32).

Dynamic Range of the Surface

In order to determine the dynamic response of the IgG assay on the developed PS surface, plasma samples spiked with different levels of RIgG-FITC conjugate were incubated with chips that were arrayed with a-RIgG. Each array was scanned and the corresponding fluorescence data were compiled in Fig. 7, demonstrating a limit of detection of 1 p*M*, and the assay reached saturation at a level of 10 n*M*. The inset images in Fig. 7 show the actual raw scans of the microarrays.

This is a significant improvement compared to our previous studies (20), where we reported a 100 p*M* detection limit. This may be explained largely by the improved detection procedure. The use of a confocal microscope scanner with high numerical aperture objective (20x oil immersion objective) dramatically improved the readout performance, compared to previous use of a CCD camera detection with a 20x air standard objective. The dynamic curve shows that the developed substrate can be used for analysis in wide range of target analyte concentrations.

Application of Macro/Nano-Structured Silicon to a Bioassay for Prostate Specific Antigen

As a first effort to evaluate the detection limit and dynamic range in a setting relevant to future clinical applications with the new porous silicon protein microarray surface, we analyzed fluorescence (FITC) labeled PSA added at concentrations ranging from 0.7 to 7 ng/mL to serum. Monoclonal IgG 2E9 specific for PSA (31) were arrayed on the porous silicon protein chip surface and the chips were processed according to the specified protocol. We measured PSA recovery in serum samples containing FITC-labeled PSA by a commercial immunoassay (Prostatus Dual Free/Total PSA from Perkin-Elmer, Turku, Finland) showing ≈70% recovery relative to the amounts of FITC-labeled purified PSA added to female blood—a recovery consistent with use of mainly non-catalytic multichain PSA forms (33). Antibody-activated PS chips were incubated with serum and were subsequently scanned in the fluorescence confocal set-up. Extracts of these findings are shown in Figs. 8 A–C, where A represents the current limit of detection (three times noise level) at approx 0.7 ng/mL (26 p*M*), B shows signal intensities at ≈70 ng/mL (2.6 n*M*), and C is signal intensities at
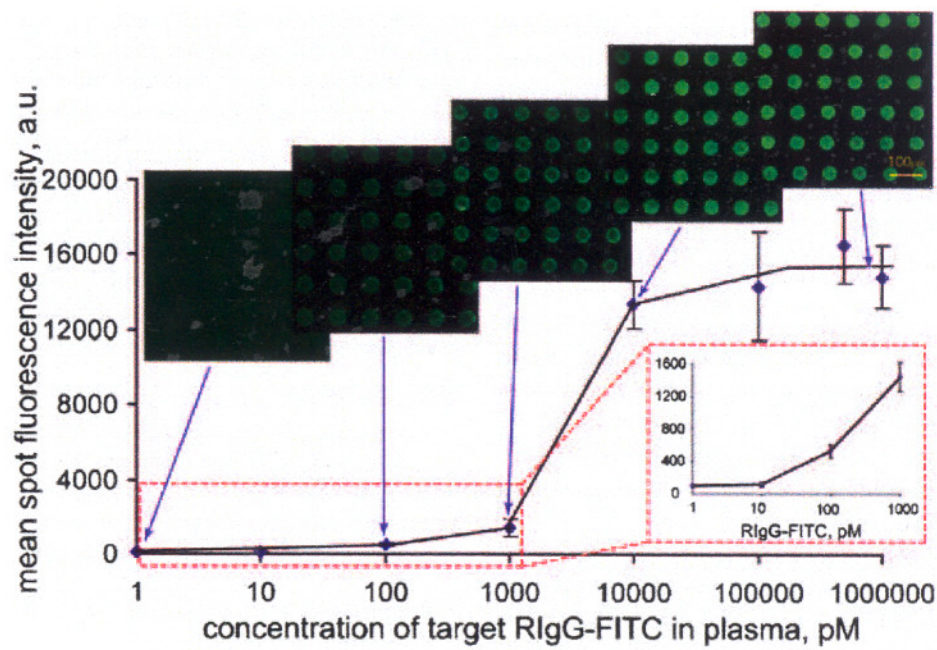
Fig. 7. Dynamic curve of the assay; 140 amol of aRIgG were spotted on the chips per each position. The chips were incubated with human plasma spiked to different levels of target RIgG-FITC.
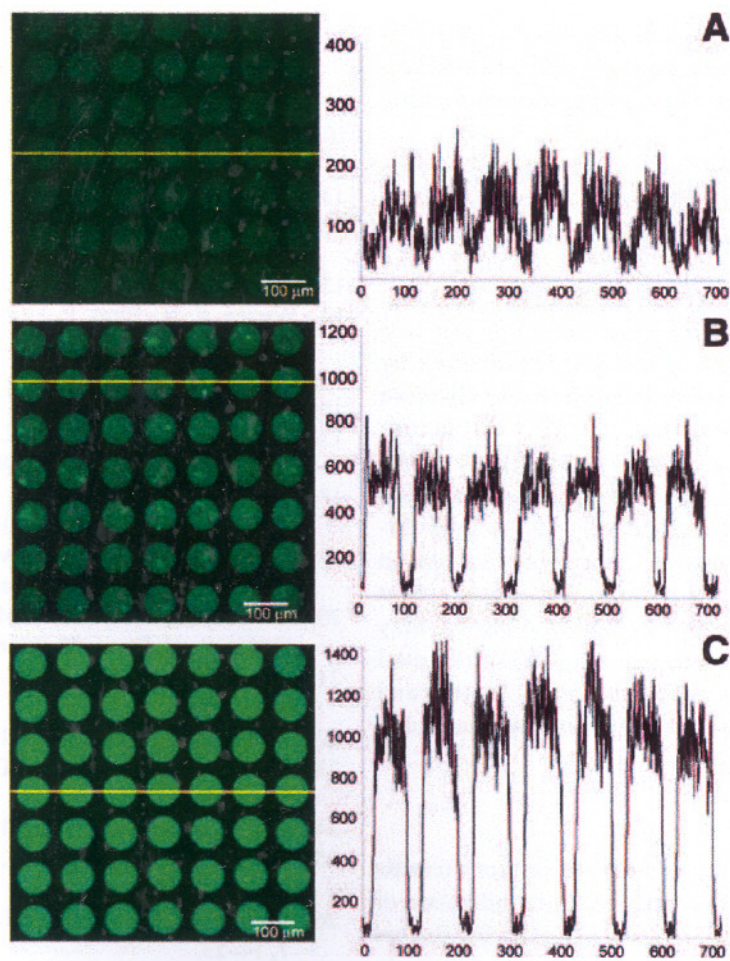

Fig. 8. (A) PSA assay in blood serum spiked with 26 pM (≈ 700 pg/mL) FITC-labeled PSA; **(B)** 2.6 nM (≈70 ng/mL), FITC-labeled PSA in blood serum; **(C)** 260 nM (≈7 µg/mL) FITC-labeled PSA in blood serum. Cross-section scans along yellow line in the corresponding (left) microarray images.

≈7 μg/mL (260 n*M*). Images (left side) show unfiltered fluorescence scans of the chips and the corresponding diagrams on the right show intensity profiles determined along the yellow line in the microarray image. No image processing or noise reduction has been employed. In regards to the issues earlier discussed on the homogeneous surface coverage of the arrayed antibody due to the tailored micro- and nanomorphology, this is again clearly illustrated in the scanned images.

The data obtained in the current study demonstrates that both limit of detection (≈0.7 ng/mL PSA) and dynamic range (10^3–10^4-fold) of our novel high-density protein chip surface correspond to those required to allow for discrimination of men with very early signs of either malignant or benign prostate disease conditions, as judged from population-based geometric mean PSA levels in serum *(34)*.

The reproducible performance of the protein microarray chips and the possibility of batch-scale chip production provide a generic platform for large-scale implementation in bioanalytical research. As demonstrated in the PSA-detection experiments performed with serum samples (i.e., a biological fluid with highly complex composition) spotted onto the protein chips, strongly imply that the proposed PS microarray platform may offer versatile and important opportunities to search for novel biomarkers in clinical diagnostics, where reproducible performance of the chip surface is a fundamental criterion.

The macro/nanoporous surface further offers the possibility to serve as a substrate for direct analysis of antibody captured antigen by means of laser desorption time of flight mass spectrometry (MALDI TOF-MS) *(17)*. The possibility to run a primary screen of the protein chip using fluorescence readout to identify positions with positive binding events and subsequently analyze these spots by MALDI TOF-MS opens the route to confirm the absolute molecular structure of the bound antigen. This will in turn enable the identification of homologs with affinity to the antibody used and also to discriminate from non-targeted biomolecules that yet display an affinity to the immobilized antibody. In our further effort to screen for kallikrein gene products that can serve as biomarkers for malignant prostate disease, the presented protein chip platform may serve as both the screening platform employing the dual readout mode (fluorescence and mass spectrometry) and in a later stage also serve as the substrate for multiplex antibody panels.

Conclusions

The developed micro/nanoporous silicon surface presents a high-surface-area 3D matrix for efficient immobilization of antibodies. Reproducible manufacturing and assaying further establishes the new surface as a strong alternative for use in protein chip applications.

The performance of the surface was demonstrated in an IgG assay reaching a detection level of 1 p*M*. The protein chip also demonstrated detection dynamics at levels of 20–30 p*M* (≈0.7 ng/mL) for PSA in blood serum, which is far below the reference limit, for 4 ng/mL). These data pave the way to implement multiplex assays in a microarray format on the new protein chip surface. Future efforts will also target the optimization of the protein chip surface and assay for direct MALDI TOF-MS readout, enabling both affinity interaction readout by fluorescence and molecular structure readout by means of mass spectrometry.

References

1. Aebersold, R. and Mann, M. (2003), *Nature* **422**, 198–207.
2. Anderson, N. L. and Anderson, N. G. (1998), *Electrophoresis* **19**, 1853–1861.
3. Goodlett, D. R., Timperman, A., et al. (2000), in *Proteome and Protein Analysis*, Choli-Papadopoulou, T., ed., Springer, Berlin, pp. 3–14.
4. Patterson, S. D. and Aebersold, R. H. (2003), *Nat. Gen.* **33**, (Suppl.), 311–323.
5. Western, A. D. and Hood, L. (2004), *J. Proteome Res.* **3**, 179–196.
6. Templin, M. F., Stoll, D., Schwenk, J. M., Potz, O., Kramer, S., and Joos, T. O. (2003), *Proteomics* **3**, 2155–2166.
7. MacBeath, G. and Schreiber, S. L. (2000), *Science* **289**, 1760–1763.
8. Zhu, H., Bilgin, M., Banghan, R., et al. (2001), *Science* **293**, 2101–2105.
9. Zhu, H. and Snyder, M. (2001), *Curr. Opin. Chem. Biol.* **5**, 40–45.
10. Kusnezow, W. and Hoheisel, J. D. (2002), *BioTechniques* **33**, S14–S23.
11. Kusnezow, W. and Hoheisel, J. D. (2003), *J. Mol. Recog.* **16**, 165–176.
12. Cretich, M., Pirri, G., Darnin, F., Solinas, I., and Chiari, M. (2004), *Anal. Biochem.* **332**, 67–74.
13. Lahann, J., USA Patent No. 2003054515 (2003).
14. Warren, E. N., Elms, P. J., Parker, C. E., and Borchers, C. N. (2004), *Anal. Chem.* **76**, 4082–4092.
15. Yu, W., Gu, N., et al. (2004), *Sens. Act. B* **98**, 83–91.
16. Zhou, Y., Andersson, O., et al., (2004), *Microchim. Acta* **147**, 21–30.
17. Finnskog, D., Ressine, A., Laurell, T., and Marko-Varga, G. (2004), *J. Proteome Res.* **3**, 988–994.
18. Deegan, R. D., Bakajin, O., Dupont T., F., Huber, G., Nagel S. R., and Witten T. A. (2000), *Phys. Rev. E* **62**, 756–765.
19. Deegan, R. D., Bakajin, O., Dupont, T. F., Huber, G., Nagel S. R., and Witten, T. A. (1997), *Nature* **389**, 827–829.
20. Ressine, A., Ekstrom, S., Marco-Varga, G., and Laurell, T. (2003), *Anal. Chem.* **75**, 6968–6974.
21. Herino, R., Bomchil, G., et al. (1987), *J. Electrochem. Soc.* **134**, 1994–2000.
22. Drott, J., Rosengren, L., et al. (1998), *Thin Sol. Film.* **330**, 161–166.
23. Cullis, A. G., Canham, L. T., et al. (1997), *J. App.Phys.* **82**, 909–965.
24. Lin, T. L. and Wang, K. L. (1986), *Appl. Phys. Lett.* **49**, 1104.
25. Ekström, S., Onnerfjord, P., Nilsson, J., et al. (2000), *Anal. Chem.* **72**, 286–293.
26. Drott, J., Lindstrom, K., et al. (1997), *J. Micromech. Microeng.* **7**, 14–23.
27. Ekins, R., Chu, F., and Biggart, E. (1990), *Ann. Biol. Clin.* **48**, 655–666.

28. Ekins, R. P. (1998), *Clin. Chem.* **44,** 2015–2030.
29. Bengtsson, M., Ekstrom, S., et al. (2002), *Talanta* **56,** 341–353.
30. Hermanson, G. T., Mallia, K. A., et al. (1992), *Immobilized Affinity Ligand Techniques,* Academic Press, San Diego.
31. Lilja, H., Christensson, A., Dahlen, U., et al. (1991), *Clin. Chem.* **37,** 1618–1625.
32. Cheek, B. J., Steel, A. B., Torres, M. P., Yu, Y. Y., and Yang, H. (2001), *Anal. Chem.* **73,** 5777–5783.
33. Christensson, A., Laurell, C. B., and Lilja, H. (1990), *Eur. J. Biochem.* **194,** 755–763.
34. Oesterling, J. E., Jacobsen, S. J., and Coosen, W. H. (1995), *J. Urol.* **154,** 1090–1095.

David Finnskog[1]
Kerstin Jaras[2]
Anton Ressine[1]
Johan Malm[2]
György Marko-Varga[3]
Hans Lilja[2, 4]
Thomas Laurell[1]

[1]Department of Electrical
 Measurement,
 Lund University,
 Lund, Sweden
[2]Department of Laboratory Medicine,
 Division of Clinical Chemistry,
 Lund University,
 University Hospital (UMAS),
 Malmö, Sweden
[3]Department of Analytical Chemistry,
 Lund University,
 Lund, Sweden
[4]Departments of Clinical Laboratories,
 Urology, and Medicine,
 Memorial Sloan-Kettering Cancer
 Center,
 New York, NY, USA

Research Article

High-speed biomarker identification utilizing porous silicon nanovial arrays and MALDI-TOF mass spectrometry

Speed and accuracy are crucial prerequisites in the application of proteomic methods to clinical medicine. We describe a microfluidic-based nanovial array for rapid proteolytic processing linked to MALDI-TOF MS. This microscale format consumes only minute amounts of sample, and it is compatible with rapid bioanalytical protocols and high-sensitivity readouts. Arrays of vials (300 μm in diameter and 25 μm deep), isotropically etched in silicon wafers were electrochemically porosified. Automated picoliter microdispensing was employed for precise fluid handling in the microarray format. Vials were prefilled with trypsin solution, which was allowed to dry. Porosified and nonporosified nanovials were compared for trypsin digestion and subsequent MS identification of three model proteins: lysozyme, alcohol dehydrogenase, and serum albumin at levels of 100 and 20 fmol. In an effort to assess the rapid digestion platform in a context of putative clinical applications, two prostate cancer biomarkers, prostate-specific antigen (PSA) and human glandular kallikrein 2 (hK2), were digested at levels of 100 fmol (PSA), 20 fmol (PSA) and 8 fmol (hK2). All biomarker digestions were completed in less than 30 s, with successful MS identification in the porous nanovial setting.

Keywords: High-speed digestion / MALDI-TOF MS / Nanovial arrays / Porous silicon / Trypsin digestion   DOI 10.1002/elps.200500751

1 Introduction

The fast acceleration of research in the area of proteomics requests new compact and rapid approaches for protein analysis. Peptide mass fingerprint mapping has become one of the predominant methods for the identification of proteins and the determination of post-translational modifications [1, 2]. The protein of interest is digested by a proteolytic enzyme, most often trypsin, and the peptides in the resulting mixture are identified using MS. An important issue in the current proteomic protocols is to reduce the relatively long time span requested for protein digestion. Minimizing this time span is the focus of the current paper. Further, access to highly limited amounts of biological samples, as well as occurrence of the target protein(s) at very low levels in this sample, infer that there are severe challenges to access sufficient amounts of the biological target to enable structural identification. Therefore, new protocols requiring only minute analyte volumes are widely sought. Microsystems are considered a fruitful way forward, in line with contemporary trends in clinical biomarker research and in clinical diagnostics. New assays in miniaturized formats are particularly valuable for validating new biomarkers among a larger panel of candidate biomarkers. Recently, enormous efforts have been directed at the development of new micro-fabricated analytical devices and their integration to create micro-total analysis systems (μTAS). Such systems aim at increased throughput, lower sample and reagent consumption, smaller overall size, and lower operating costs than full-size instrumentation [3, 4]. This has earlier been reported for well-established analytical techniques, such as electrophoresis [5–7], electrochromatography [8–11], assays involving enzymes [12–16], and immunoassays [17–19].

Speed and accuracy are prerequisites for applying proteomic research methods in clinical medicine. To validate the clinical usefulness of novel technology, analysis of

Correspondence: Professor Thomas Laurell, Department of Electrical Measurement, Lund University, Box 118, S-221 00 Lund, Sweden
E-mail: Thomas.Laurell@elmat.lth.se
Fax: +46-46-222-45-27

disease biomarkers is a key assignment. In this study, the reported improved nanovial digestion protocols were thus validated on prostate cancer biomarkers. Prostate cancer is the most common cancer in males in Western Europe and the USA, and also a major cause of death. While measurements of prostate-specific antigen (PSA) in plasma give a good indication of prostate disease, concerns about diagnostic specificity have been voiced. Only 25% of men with slightly elevated PSA levels do have prostate cancer. Approximately the same percentage of males with PSA levels in the upper normal range do indeed have prostate carcinoma, though it is often not possible to distinguish between consequential and nonconsequential tumors. In addition, a large number of prostate cancer patients die with the disease, and not from it, indicating the disease complexity. Thus, we must now move beyond using PSA for detection of prostate carcinoma to a detection strategy that incorporates disease prognosis.

Kallikrein 3, commonly known as PSA, is the most widely used serum biomarker to distinguish between benign and malignant prostatic disease. All cancers considered, PSA is the most valuable of all tumor markers. It is used for both diagnosis and to monitor patients with established cancer. Several studies [20, 21] have also identified human kallikrein 2 (hK2) as a potential serum marker of prostate carcinoma. Both PSA and hK2 belong to the kallikrein gene family, located on chromosome 19q13.3-13.4 [22, 23]. The gene products of the kallikrein family are all putative serine proteases. The enzyme activity of PSA is mainly directed to semenogelin I, II and fibrinogen [24–27], in order to induce liquefaction of semen and subsequent release of motile spermatozoa. Transcribed hK3 is an inactive pre-pro-PSA-precursor, a common feature among serine proteases. During the secretory pathway, the signal peptide of 17 amino acids is released, and pro-PSA formed. This zymogen form of PSA (244 amino acids) is, according to three studies [28–30], converted to active PSA (237 amino acids) by hK2 *in vitro.* The findings might suggest a possible connection between PSA and hK2 *in vivo*.

In clinical routine PSA and hK2 are measured using immunoassays. Despite recent advances within the research area, the need for novel technologies allowing rapid analysis in miniaturized formats is tremendous. A miniaturized technique would allow higher throughput, decrease time consumption and diminish both analyte and sample volume. The molecular masses of the kallikreins, around 26 kDa based on amino acid sequence [31], are large enough to produce peptides for a satisfactory MS identification. In line with these requirements MS is a strong candidate from the analytical point of view.

However, when performing protein analysis using MS the preceding protein digestion step over hours is commonly a major bottleneck from the high-throughput perspective. In order to address this issue, miniaturized protein digestion protocols have been developed, showing efficient cleavage of proteins at low femtomolar level in less than 60 s [32]. These data were generated in nanovials with a diameter of a few hundred micrometers with a volume capacity in the nanoliter range, providing excellent reaction vessels for high-speed enzymatic reactions [33]. This improved catalytic efficiency is due to continuous solvent evaporation during the dispensing of substrate into the vials, which generates an increased substrate concentration that drives the formation of enzyme–substrate complexes according to the Michaelis-Menten kinetics (1), illustrated in Fig. 1. In Eq. (1), the substrate concentration is denoted [S], the maximal turnover rate V_{max}, and the substrate concentration at which the reaction rate is half of its maximal value K_M.

$$V = V_{max} \frac{[S]}{[S] + K_M} \qquad (1)$$

It can be anticipated that the increased surface area to volume ratio in these nanovials further promotes proteolytic turnover, as a larger proportion of the enzyme-target protein interaction occurs on the solid surface when the vial dimensions are reduced. This was further demonstrated in reports on protein microdigestion [34, 35]. Data reported in this paper also support this hypothesis, showing that protein digestion using unbound enzymes in nanovials manifests sufficient protein digestion in 10–15 s at low femtomolar level.

In an effort to increase the surface area available in the nanovials, and hence further accelerate the digestion protocol, we electrochemically created a porous silicon (PS) layer in the nanovial in order to combine the nanovial format with a highly surface-enlarging approach.

This paper demonstrates the improved proteolytic efficiency when the target proteins are digested in porosified nanovials. Digestion protocols were developed on model systems of lysozyme, alcohol dehydrogenase (ADH), and serum albumin. The nanovial arrays also served as an MS target enabling direct readout of the peptide mass fingerprint after automated matrix microdispensing into the nanovial array. The corresponding protocols were subsequently used in the identification of two prostate cancer biomarkers, PSA and hK2. The results from nanovials, both with and without PS, were studied, and the characteristic peptides from the two kallikreins were identified at protein levels below 10 fmol.
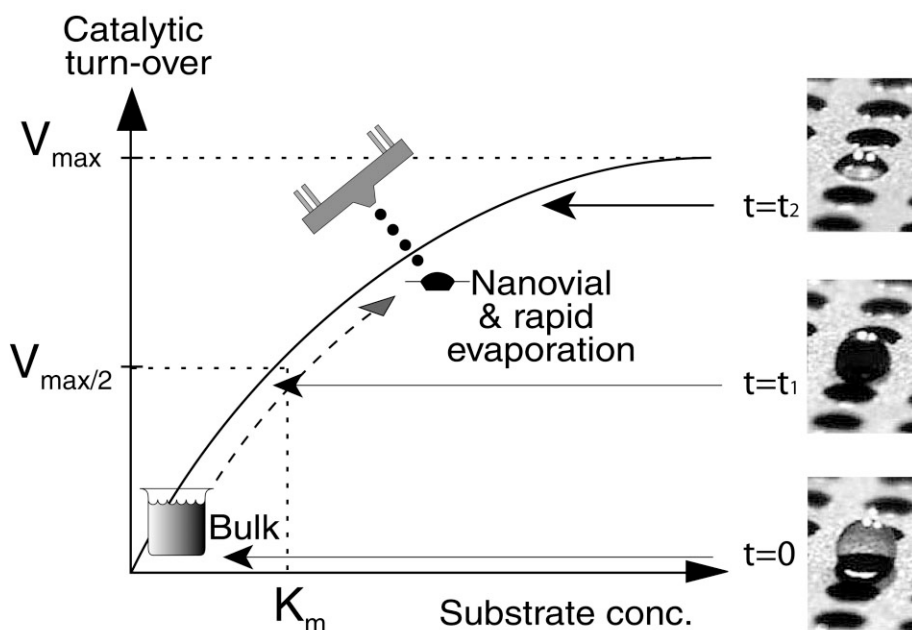
Figure 1. Schematic over the accelerated enzyme kinetics due to the substrate enrichment as the solvent evaporates from the nanovial. V_{max} is the maximal turnover rate independent of substrate concentration and K_M is equal to the substrate concentration at which the reaction rate is half of its maximal value. $t = 0$, enzyme kinetics rules due to bulk solution stoichiometry; $t = t_1$, substrate enrichment increases the enzymatic turnover due to solvent evaporation; $t = t_2$, maximum substrate enrichment properties have been reached, and surface area to volume ratio becomes dominant. Hence, surface-bound catalysis further accelerates the digestion process.

2 Materials and methods

2.1 Proteins

Lysozyme C (LyC) from chicken egg white, ADH from bakers yeast, and BSA were all obtained from Sigma (St. Louis, MO, USA). PSA was purified from human seminal plasma with immunoaffinity chromatography using four monoclonal anti-PSA antibodies, 2E9, 5A10, 2C1, and 2H11, coupled to Affigel 10 from BioRad (Hercules, CA, USA). The eluted protein solution was further purified by gel filtration (Sephacryl S-200 HR, Pharmacia Biotech, Uppsala, Sweden), and size and purity were confirmed by SDS-PAGE and Western blot. Recombinant hK2 (fXahK2) was produced by baculovirus expression system using the Bac-to-Bac system (Gibco, Life Technologies). The virus stocks *Ac*fXahK2 were produced in *Spodoptera frugiperda* (Sf9) cells, and the proteins generated in *Trichoplusia ni* (Hi Five™) cells. The cultivation/infection methods used were essentially the ones described in the Bac-to-Bac Baculovirus Expression System manual. Immunoaffinity chromatography with monoclonal anti-hK2 antibody 11B6 was performed for purification of fXahK2. Size and purity were confirmed by SDS-PAGE and Western blot. Before dispensing the protein, fXahK2 was extensively dialyzed against 10 mM ammonium bicarbonate (NH_4HCO_3) buffer, using Slide-A-Lyzer MINI Dialysis Units (Pierce, Rockford, IL, USA), with a 3.5 kDa MW cutoff. Trypsin was of proteomics grade and bought from Sigma. ADH, BSA, and PSA were dissolved to concentrations of 40 and 8 μM each in 10 mM

NH_4HCO_3 buffer (pH 7.8) without any reduction or alkylation. hK2 concentration was 3.2 μM. For protein digestions, trypsin was used in a concentration of 5 μM in 10 mM NH_4HCO_3 buffer, pH 7.8.

2.2 Buffers, protein reduction, and alkylation

Iodoacetamide (IAA), DL-DTT (DTT), and NH_4HCO_3 were from Sigma. Before enzymatic digestion, LyC was subjected to reduction and alkylation to facilitate digestion. The protein was reduced in 1.5 mL Eppendorf© tubes with 15 mM DTT to 40 μM LyC in 10 mM NH_4HCO_3 buffer pH 7.8 at 50°C for 45 min. Thereafter, to alkylate the reduced cystein residues, IAA was added to a concentration of 50 mM for at least 1 h in dark at room temperature.

2.3 Matrices, chemicals, and mass calibrators for MALDI-TOF analysis

α-Cyano-4-hydroxycinnamic acid (α-CHCA) 99% and TFA 99%+ were bought from Sigma. ACN was purchased from Fluka (Germany). Isopropanol 99%+ was from Acros Organics (Geel, Belgium). All water used was purified and deionized by a Millipore apparatus with nylon membrane filter (Bedford, MA, USA). Internal standard solution was prepared by dissolving the peptide fragment ACTH 18–39 from Sigma in 50% ACN, 0.1% TFA, 49.9% water v/v/v to a concentration of 10 pmol/μL.

Matrix solution was prepared by dissolving α-CHCA at 5 mg/mL in 50% ACN, 0.1% TFA, 49.9% water v/v/v. To the matrix solution were added 5% isopropanol, to avoid clogging of the dispenser, and 2–5% of internal standard.

2.4 Microdispenser made from silicon

The construction and proteomic applications of the microdispenser have been described in previous publications [36–38]. In the earlier work of Ericsson *et al.* [32] the dispenser was, however, not used for matrix application on the dried digest because rapid solvent evaporation caused matrix crystallization in the dispenser orifice. The addition of 5% isopropanol to the matrix solution (as described in Section 2.3) prevented the crystallization and enabled use of the microdispenser for matrix application. The dispenser was mounted over an *x,y*-stage manufactured in-house, and droplet dispensing was supervised using close-up optics mounted on a CCD camera (Hamamatsu C5403, Shizouka, Japan), connected to a 14 in. monitor.

2.5 MALDI-TOF MS

The MALDI-TOF mass spectrometer used was a Micromass Matilda II (Micromass, Manchester, UK). It was equipped with a delayed extraction ion source, utilized a nitrogen laser at 337 nm, and was operated in reflection mode at an accelerating voltage of 20 kV. Further, the instrument was equipped with a video camera to make it possible to find and focus the laser beam onto the nanovials.

2.6 Porous nanovials

The silicon used for nanovial production was obtained from Siltronix (USA), crystal orientation <110>, and resistivity 10–50 Ω/cm. All chemicals used for isotropic etching, HNO_3:HF:CH_3COOH (8:1:3 v/v/v) as well as for porosification HF:DMF (1:10 v/v), were from Merck (Darmstadt, Germany).

Vials were isotropically etched for 25 min, giving vials with a depth of 25 μm and a diameter of 300 μm. The chip was subsequently porosified under backside illumination as described in detail earlier [17]. This resulted in a chip of 20×20 mm^2 with a circular porosified area, 14 mm in diameter and containing a total of 370 porous vials. Nonporous vials were used as a reference to compare digestion rates.

3 Results and discussion

By reducing the reaction volume, reaction kinetics are increased due to concentration dependency [39]. This is especially important when dealing with extremely small or expensive amounts of starting material. Another aspect is time. Since contemporary proteomic labs are frequently automated with a high throughput of samples, it is desirable to reduce digestion time from hours to minutes or even seconds. In general, digestion efficiency is known to be significantly more effective when the concentration of protein is increased to micromolar levels or higher. The reason for this is that proteases, such as trypsin, manifests 50% of the maximal activity in the 5–50 μM range of substrate [40]. It has been demonstrated that the digest speed in vials is related to the available surface area, [39] which also explains the increased digestion speed in nanovials as the surface area to volume ratio increases with reduced vial dimensions, as earlier reported by Ericsson *et al.* [32].

3.1 Dispensing into nanovials

A microdispenser station is essential for the nanovial digestion protocols described in this work (Fig. 2). Liquid handling of the matrix solution has previously been a limiting factor, because α-CHCA solution dissolved in 50% ACN frequently crystallized in the dispenser nozzle. However, we found that the addition of 5% isopropanol in
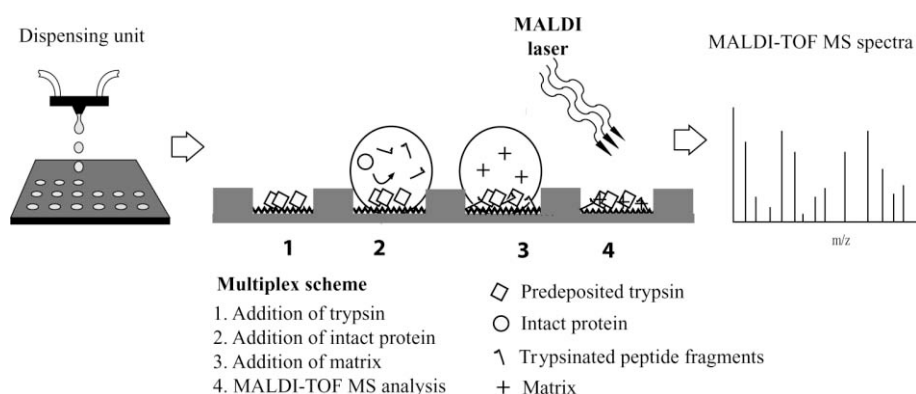

Figure 2. Schematic of the high-speed protein digestion protocol, starting with (1) microdispenser-based deposition of the enzyme; (2) dispensing of protein solution, evaporation, and increased digestion rate; (3) dispensing of MALDI matrix; and (4) laser desorption ionization and MS readout.

the matrix solution prevented the crystallization by slowing solvent evaporation. This was a major improvement since it enabled a reproducible addition of matrix solution to the nanovials in the submicroliter quantities. The amount of matrix added was 25 droplets/vial, corresponding to a total volume of 2.5 nL.

3.2 PS nanovials

In line with the findings of increased catalytic performance in systems with higher surface area to volume ratio the current investigation of porous nanovial was an evident route to follow. Electrochemical etching was used to obtain a surface-enlarging micro/nanoporous layer on the nanovial array. Figure 3a shows a series of nanoliter aliquots and their state of evaporation. Figures 3b–e show a series of scanning electron microscope images of the nanovials, revealing the pores with a characteristic size of 1–2 μm and a pore layer thickness in the range of 7 μm.

3.3 Evaporation in nanovials

The porous nanovials were found to provide a much higher volume capacity than the nonporous nanovials, in spite of the equal geometrical nanovial proportions. This can be explained by the hydrophobic behavior of the surface in the nanovial, due to which the micro- and nanoporous morphology displays hydrophobic behavior *versus* the fluid despite a hydrophilic surface chemistry. This phenomenon is analogous to the well-known nonwetting properties of the lotus flower [41, 42]. With a higher loading capacity *per* nanovial the sample also has more time to digest the protein. In addition, evaporation time for the same volume deposited on a hydrophobic surface (PS) is more optimal in this application, providing sufficient time for digestion, as compared to a hydrophilic surface (*e.g.*, stainless steel). It is important to note that too short evaporation may not provide the requested protein cleavage time.

Evaporation times for equal fluid volumes dispensed into the porous and the nonporous nanovials are given in Fig. 4. An important aspect is also the fact that the projected area and thus the MALDI spot size in the vial in these two cases are equal, which in the case of the porous nanovial offers a higher surface concentration of peptides for MALDI analysis, due to the higher loading capacity and the longer digest time, still only being in the order of tens of seconds.

Clearly, the increased volume capacity and optimal evaporation time in the porous nanovials are beneficial for rapid on-chip digests. Earlier work on nanovial-based protein digestion has put substantial efforts into the reduction of the solvent evaporation in order to allow sufficient digestion time. The most obvious approach has been enclosure of the sample in a humidified environment [43]. However, unless humidity and temperature conditions are rigidly controlled, high humidity levels may induce condensation on the chip surface, which can cause overflow and crosscontamination between the vials.
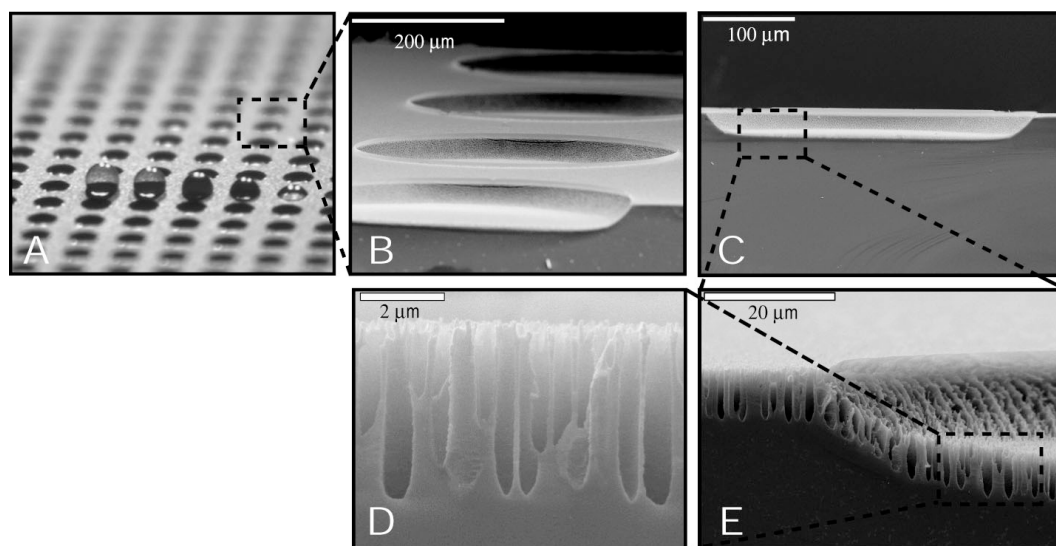

Figure 3. PS nanovials. (A) A series of aliquots sequentially dispensed in the array, (B–E) scanning electron microscope close-up images of the nanovials and the porous layer, providing the surface area enlargement.
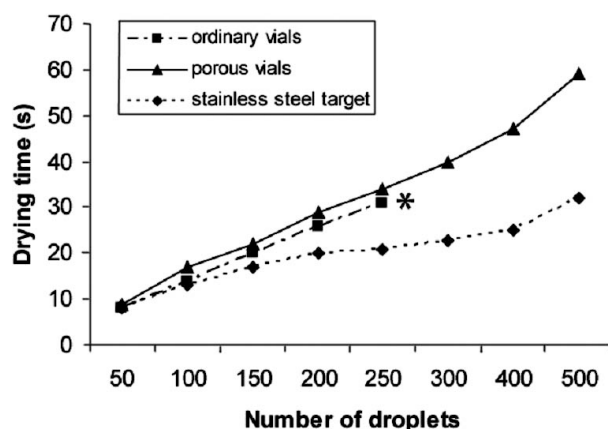
Figure 4. Drying time for dispensed droplets (deionized water) in porous and nonporous nanovials and on an ordinary MALDI stainless steel target. * indicates the highest loading capacity for a nonporous nanovial. Compared to the nonporous vial, the porous vial had twice the capacity for aqueous solution, as defined by the volume that could be dispensed before the array was flooded.

Yet another method to decrease evaporation is addition of solvents of low vapor pressure, such as glycerol [44] or triethylene glycol [45], to the digest solution. The main drawback of this technique is that these additives may be contaminants in the subsequent analytical measurements, such as MS, immunoassays, CE, *etc*. Instead of reducing the rate of evaporation it is possible to apply liquid continuously to the vials to compensate for evaporation [32, 46]. When a continuous supply of solvent is added in balance with evaporation, reactions can be sustained for several hours, so-called prolonged digestion. It is, however, of great importance to use pure and volatile solvents to avoid accumulation of, for example, salts and trace contaminants. Yet another approach reported to reduce solvent evaporation is the use of a volatile liquid lid, *e.g.*, of octane, that completely covers the digestion compartment. This approach has allowed reaction times of hours for volumes as small as 15 nL [47].

3.4 Protein digestion in porous nanovials

Our main interest was determining whether a micro-/ nano-PS nanovial would speed enzymatic kinetics compared to an equivalent vial with nonporous surface. This assumption was based on earlier work, where the introduction of a thin gold wire in a macroscaled vial [39], provided a considerably increased surface area, resulting in significantly more effective protein digestion.

It is not unreasonable to assume that the observed kinetic difference for digests performed in differently structured vials is related to microscale surface properties and their

individual surface to volume ratio. It is well known that surfaces, in general, adsorb proteins and peptides [48–51]. During surface adsorption, native protein molecules form a mainly random coil structure [49, 51]. Such conformational changes are likely to result in an increased accessibility of the enzyme to the protein. For a continued digestion process *via* surface-adsorbed proteins, the digestion products have to be exchanged with new protein molecules at the surface. This is likely to occur since it has been shown in terms of surface binding energy that proteins are preferentially adsorbed compared to peptides [52]. It has also been suggested [53, 54] that a consecutive replacement of adsorbed proteins to more surface active ones occurs even though the latter are present in lower concentrations in the solution. Other factors like the shorter diffusion length in the nanovials could also enhance the digest due to faster mass transfer-related association of protein molecules to the vial surfaces.

For digestion reactions, 12 fmol/vial of trypsin was dispensed into the vials in 25 droplets (2.5 nL), just covering the bottom of the vials, and then allowed to dry. No coupling reactions were used for the immobilization of trypsin. The digestion of three model proteins, lysozyme, ADH, BSA, and two prostate cancer biomarkers, PSA and human glandular kallikrein 2, were investigated. Figure 5 shows the resulting peptide mass fingerprint for lysozyme after 15 s digestion of either 100 fmol (top) or 20 fmol (lower) as compared to the corresponding digestions performed in nonporous nanovials. Identified peptides are marked with a star. Figure 6 shows the corresponding digestion data for ADH, digested for 90 s, and Fig. 7 holds the digestion data for BSA, digested for 15 s.

Peptide mapping was done using MASCOT search for peptides in the mass range of 800–3000 Da. The numbers of matched peptides as a percentage of theoretical peptides are presented in Fig. 8. For all three proteins at both concentration levels, these percentages were higher for porous nanovials compared to nonporous nanovials. Thus, the porous nanovials offered clearly superior analytical performance for all the model proteins investigated.

3.5 Analysis of prostate cancer biomarkers

To validate the clinical usefulness of rapid on-chip digestion, the prostate cancer biomarkers, PSA and hK2, were analyzed on the nanovial platform. In the MALDI-TOF spectra of 100 and 20 fmol PSA, five and three characteristic peptides were identified, respectively (Fig. 9). The peptides were matched to the amino acid sequence, and marked bold and underlined (Fig. 10). In the hK2 experiment the detection limit was further improved to below 10 fmol. Four peptides were identified (Figs. 11, 12). The
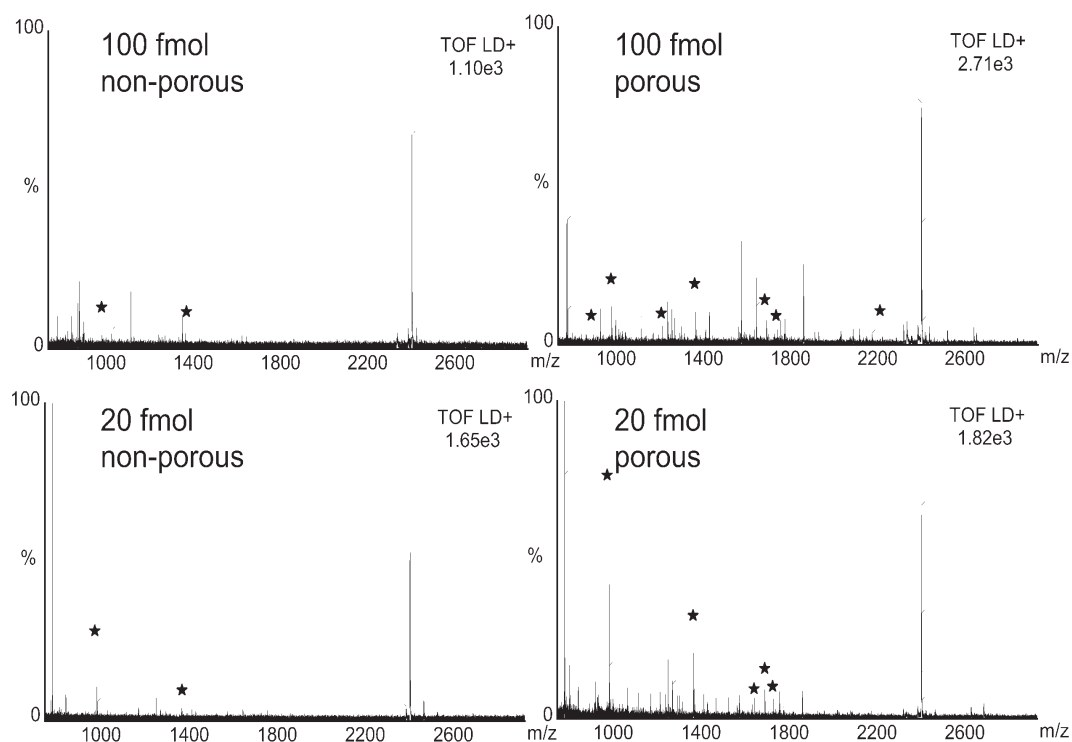
Figure 5. Lysozyme digested for 15 s in quantities of 100 fmol (top) and 20 fmol (bottom). Vials used were nonporous (left) and porous (right).
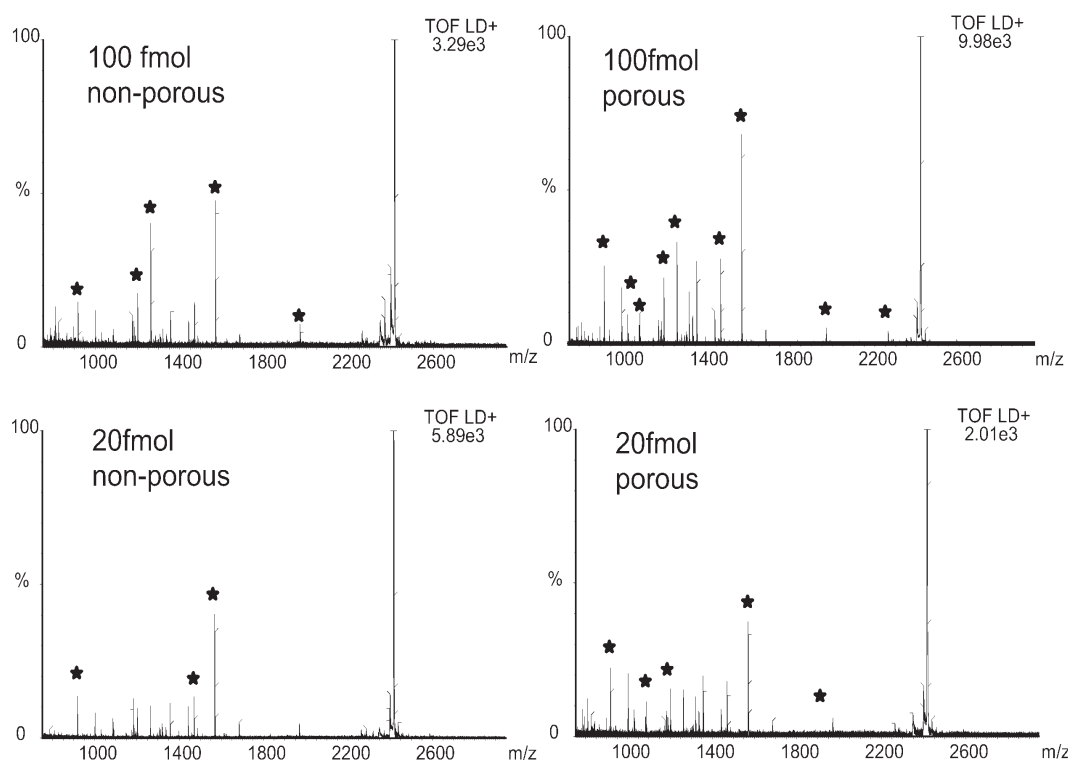
Figure 6. ADH digested for 90 s in quantities of 100 fmol (top) and 20 fmol (bottom). Vials used were nonporous (left) and porous (right).
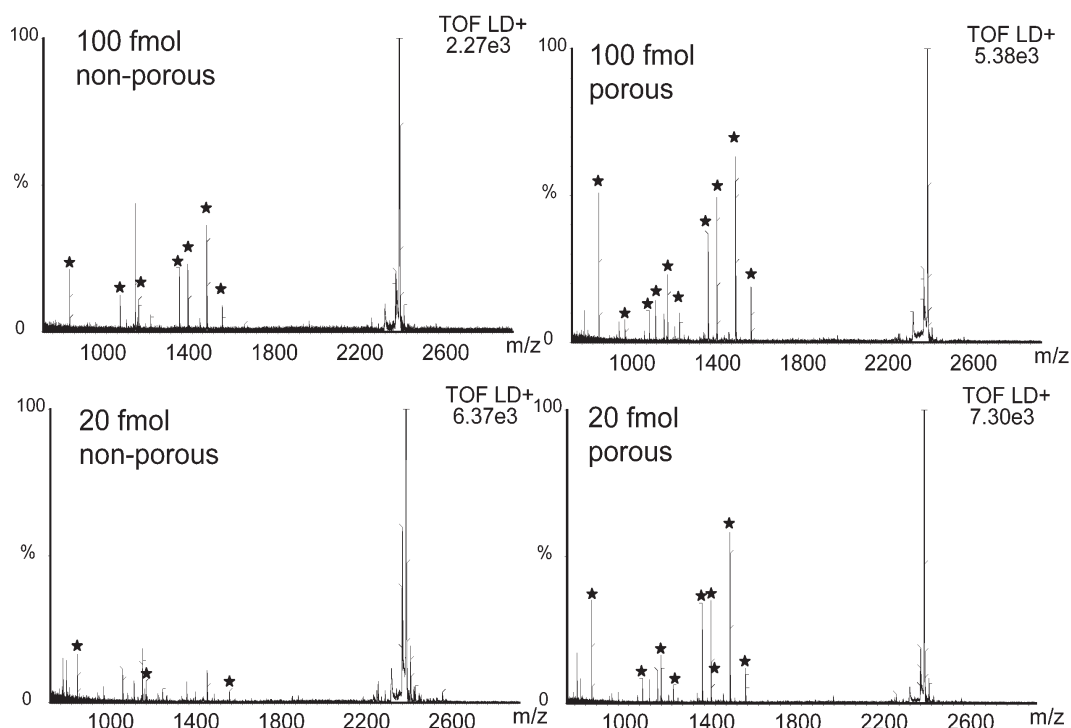
Figure 7. BSA digested for 15 s in quantities of 100 fmol (top) and 20 fmol (bottom). Vials used were nonporous (left) and porous (right).
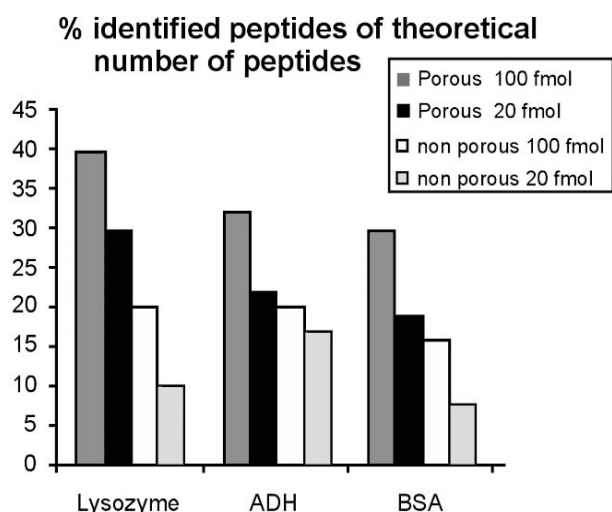

Figure 8. Relation of identified peptides to theoretical peptides for the studied proteins after accelerated nanovial digestion. In general more peptides were identified in the porous vials.

1442.7-peak, in particular, seemed to be highly indicative of the biomarker. Interestingly, the hK2 peptide 2149.0 (amino acids 108–125) and the PSA peptide 1871.9 (amino acids 110–125) were both present in the spectra.

These peptides have more than 80% sequence identity, and they are probably easily accessible to trypsin. The hK2 peptide pattern differed from that produced by an Eppendorf tube digestion of hK2 with trypsin (data not shown). This finding indicates that the protein might change conformation, when adsorbed to the PS surface, and new cleavage sites become accessible.

The MALDI-TOF spectra of the porous nanovials demonstrated a higher frequency of identified peptides, and better S/N, compared to the non-PS vials, which correlates very well with the findings on model proteins. In addition, there seemed to be a tendency of better ionization from the porous layer, since more successful spectra were generated. This might indicate a better matrix crystallization, due to the area enlargement, but also due to the fine structure of the PS. Better matrix crystallization has earlier been reported by adding tryptic peptides and matrix onto a seed layer of diluted matrix [55]. Perhaps the PS could serve as an alternative to the seed layer. However, this hypothesis needs to be further investigated. A plausible explanation to the higher signal would be if the PS simultaneously functions as a surface for desorption/ionization on silicon (DIOS) in accordance with earlier findings by Siuzdak and co-workers [56, 57].
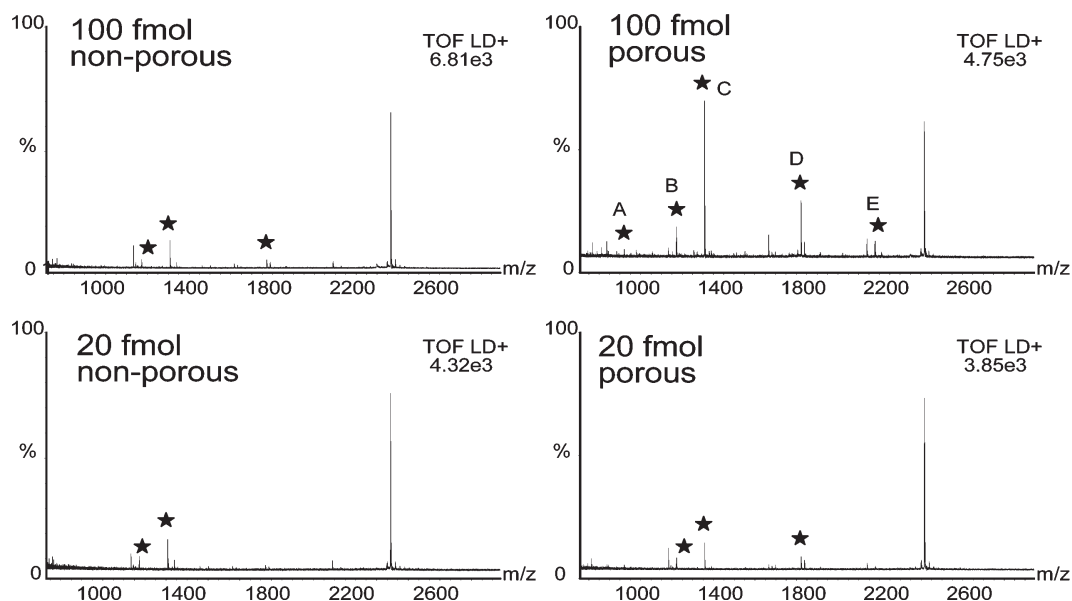
Figure 9. PSA digested for 15 s in quantities of 100 fmol (top) and 20 fmol (bottom). Vials used were nonporous (left) and porous (right).

```
            10          20          30          40
MWVPVVFLTL  SVTWIGAAPL  ILSRIVGGWE  CEKHSQPWQV

            50          60          70          80
LVASRGRAVC  GGVLVHPQWV  LTAAHCIRNK  SVILLGRHSL

            90         100         110         120
FHPEDTGQVF  QVSHSFPHPL  YDMSLLKNRF  LRPGDDSSHD

           130         140         150         160
LMLLRLSEPA  ELTDAVKVMD  LPTQEPALGT  TCYASGWGSI

           170         180         190         200
EPEEFLTPKK  LQCVDLHVIS  NDVCAQVHPQ  KVTKFMLCAG

           210         220         230         240
RWTGGKSTCS  GDSGGPLVCN  GVLQGITSWG  SEPCALPERP

           250         260
SLYTKVVHYR  KWIKDTIVAN  P
```

Figure 10. Amino acid sequence of PSA. Bold, under-lined amino acids constitute the peptides identified in the mass spectrum. Peptide A (1020.5) corresponds to amino acids 25–33, B (1272.7) to amino acids 126–137, C (1407.7) to amino acids 34–45, D (1871.9) to amino acids 110–125, and E (2230.2) to amino acids 48–68.
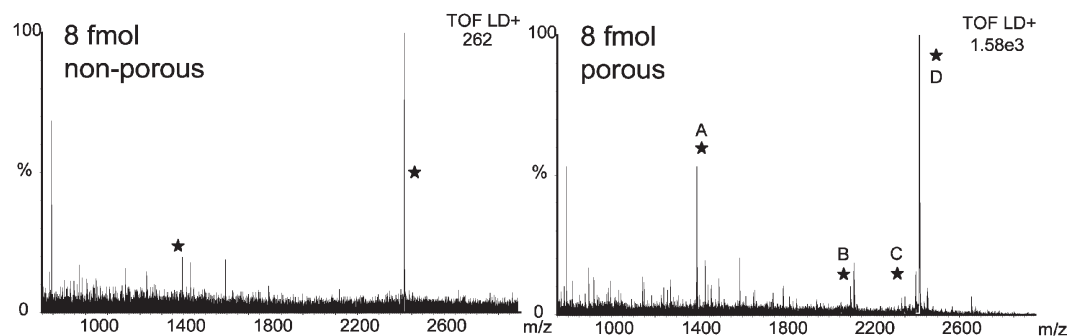

Figure 11. hK2 digested for 30 s in quantities of 8 fmol. Vials were nonporous (left) and porous (right).

　　　　　　　　　　　　　www.electrophoresis-journal.com

```
         10         20         30         40
MWDLVLSIAL SVGCTGAVPL IQSRIVGGWE CEKHSQPWQV

         50         60         70         80
AVYSHGWAHC GGVLVHPQWV LTAAHCLKK**N SQVWLGRHNL**

         90        100        110        120
**FEPEDTGQR**V PVSHSFPHPL YNMSLLK**HQS LRPDEDSSHD**

        130        140        150        160
**LMLLR**LSEPA KITDVVKVLG LPTQEPALGT TCYASGWGSI

        170        180        190        200
EPEEFLRPR**S LQCVSLHLLS NDMCARAYSE K**VTEFMLCAG

        210        220        230        240
LWTGGKDTCG GDSGGPLVCN GVLQGITSWG PEPCALPEKP

        250        260
AVYTKVVHYR KWIKDTIAAN P
```

Figure 12. Amino acid sequence of human glandular kallikrein 2. Bold, underlined amino acids constitute the peptides identified in the mass spectrum. Peptide A (1442.7) corresponds to amino acids 78–89, and B (2149.0) to amino acids 108–125. Two peptides include a missed cleavage site: C (2383.2) and D (2468.2), corresponding to amino acids 70–89 and 170–191, respectively.

4 Concluding remarks

The hypothesis that higher surface area in microspace can improve proteolytic performance in proteomics studies is clearly proven in this comparative study of protein digestion in porous *versus* nonporous nanovials. We also demonstrated the potential use of porous nanovial arrays as a platform for prostate cancer biomarker identification. In clinical routine, PSA and hK2 are measured using immunoassays. A miniaturized technique would allow higher throughput, decrease the time required, and diminish both analyte and sample volume. An attractive possibility, in line with our on-going research, is combining the porous nanovials with antibody-based affinity probing (PS protein microarrays) for multiplex biomarker detection in clinical samples, where a terminal step in the analysis is a high-speed on-chip biomarker digestion followed by MALDI-TOF MS readout.

5 References

[1] Gevaert, K., Vandekerckhove, J., *Electrophoresis* 2000, *21*, 1145–1154.

[2] Lazar, I. M., Ramsey, R. S., Ramsey, J. M., *Anal. Chem.* 2001, *73*, 1733–1739.

[3] van der Berg, A., Lammerink, T. S. J., *Top. Curr. Chem.* 1998, *194*, 21–49.

[4] Bruin, G. J. M., *Electrophoresis* 2000, *21*, 3931–3951.

[5] Gao, J., Xu, J. D., Locascio, L. E., Lee, C. S., *Anal. Chem.* 2001, *73*, 2648–2655.

[6] Liu, Y. J., Foote, R. S., Jacobsson, S. C., Ramsey, R. S., Ramsey, J. M., *Anal. Chem.* 2000, *72*, 4608–4613.

[7] Wang, J., Chatrathi, M. P., Mulchandani, A., Chen, W., *Anal. Chem.* 2001, *73*, 1804–1808.

[8] Ceriotti, L., de Rooij, N. F., Verpoorte, E., *Anal. Chem.* 2002, *74*, 639–647.

[9] Ericson, C., Holm, J., Ericson, T., Hjertén, S., *Anal. Chem.* 2000, *72*, 81–87.

[10] Ngola, S. M., Fintschenko, Y., Choi, W. Y., Sheppodd, T. J., *Anal. Chem.* 2001, *73*, 849–856.

[11] Throckmorton, D. J., Schepodd, T. J., Singh, A. K., *Anal. Chem.* 2002, *74*, 784–789.

[12] Drott, J., Lindstrom, K., Rosengren, L., Laurell, T., *J. Micromech. Microeng.* 1997, *7*, 14–23.

[13] Laurell, T., Drott, J., Rosengren, L., Lindstrom, K., *Sens. Actuators* 1996, *31*, 161–166.

[14] Mao, H., Yang, T., Cremer, P. T., *Anal. Chem.* 2002, *74*, 379–385.

[15] Wang, J., *Electrophoresis* 2002, *23*, 713–718.

[16] Wang, J., Chatrathi, M. P., Tian, B. M., *Anal. Chem.* 2000, *72*, 5774–5778.

[17] Ressine, A., Ekstrom, S., Marko-Varga, G., Laurell, T., *Anal. Chem.* 2003, *24*, 6968–6974.

[18] Dodge, A., Fluri, K., Verpoorte, E., de Rooij, N. F., *Anal. Chem.* 2001, *73*, 3400–3409.

[19] Sato, K., Tokeshi, M., Kimura, H., Kitamori, T., *Anal. Chem.* 2001, *73*, 1213–1218.

[20] Becker, C., Piironen, T., Pettersson, K., Hugosson, J., Lilja, H., *J. Urol.* 2003, *170*, 1169–1174.

[21] Haese, A., Graefen, M., Becker, C., Noldus, J., *et al.*, *Prostate* 2003, *54*, 181–186.

[22] Yousef, G. M., Luo, L. Y., Diamandis, E. P., *Anticancer Res.* 1999, *19*, 2843–2852.

[23] Yousef, G. M., Diamandis, E. P., *Genomics* 2000, *65*, 184–194.

[24] Lilja, H., Oldbring, J., Rannevik, G., Laurell, C. B., *J. Clin. Invest.* 1987, *80*, 281–285.

[25] Lilja, H., Abrahamsson, P. A., Lundwall, A., *J. Biol. Chem.* 1989, *264*, 1894–1900.

[26] Lilja, H., Lundwall, A., *Proc. Natl. Acad. Sci. USA* 1992, *89*, 4559–4563.

[27] McGee, R. S., Herr, J. C., *Biol. Rep.* 1988, *39*, 499–510.

[28] Takayama, T. K., Fujikawa, K., Davie, E. W., *J. Biol. Chem.* 1997, *272*, 21582–21588.

[29] Lovgren, J., Rajakoski, K., Karp, M., Lundwall, A., Lilja, H., *Biochem. Biophys. Res. Commun.* 1997, *238*, 549–555.

[30] Kumar, A., Mikolajczyk, S. D., Goel, A. S., Millar, L. S., Saedi, M. S., *Cancer Res.* 1997, *57*, 3111–3114.

[31] Bridon, D. P., Dowell, B. L., *Urology* 1995, *45*, 801–806.

[32] Ericsson, D., Ekstrom, S., Nilsson, J., Bergquist, J., *et al.*, *Proteomics* 2001, *1*, 1072–1081.

[33] Ekstrom, S., Ericsson, D., Önnerfjord, P., Bengtsson, M., *Anal. Chem.* 2001, *73*, 214–219.

[34] Bengtsson, M., Ekstrom, S., Marko-Varga, G., Laurell, T., *Talanta* 2002, *56*, 341–353.

[35] Gobom, J., Nordhoff, E., Ekman, R., Roepstorff, P., *Int. J. Mass Spectrom. Ion Proc.* 1997, *169*, 153–163.

[36] Laurell, T., Wallman, L., Nilsson, J., *J. Micromech. Microeng.* 1999, *9*, 369–376.

[37] Miliotis, T., Kjellström, S., Nilsson, J., Laurell, T., *J. Mass Spectrom.* 2000, *35*, 369–377.

[38] Önnerfjord, P., Nilsson, J., Wallman, L., Laurell, T., *Anal. Chem.* 1998, *70*, 4755–4760.

[39] Litborn, E., Emmer, Å., Roeraade, J., *Anal. Chim. Acta* 1999, *401*, 11–19.

[40] James, P., *BioTechniques* 2002, *33*, 4–13.

[41] Barthlott, W., Neinhuis, C., *Planta* 1997, *202*, 1–8.

[42] Ressine, A., Finnskog, D., Malm, J., Becker, C., Lilja, H., Varga, G. M., Laurell, T., *NanoBiotechnology* 2005, *1*, 93–104.

[43] Oldenburg, K., Zhang, J., Chen, T., Maffia, A., Blom, K., Combs, A., Chung, T., *J. Biomol. Screening* 1998, *3*, 55–62.

[44] Hietpas, P. B., Ewing, A. G., *J. Liq. Chromatogr.* 1995, *18*, 3557–3576.

[45] Jackman, R. J., Duffy, D. C., Ostuni, E., Willmore, N. D., Whitesides, G. M., *Anal. Chem.* 1998, *70*, 2280–2287.

[46] Litborn, E., Emmer, A., Roeraade, J., *Electrophoresis* 2000, *21*, 91–99.

[47] Litborn, E., Roeraade, J., *J. Chromatogr. B* 2000, *745*, 137–147.

[48] Lindblad, M., Lestelius, M., Johansson, A., Tengvall, P., Thomsen, P., *Biomaterials* 1997, *18*, 1059–1068.

[49] Sui, S. F., Wu, H., Sheng, J., Guo, Y., *J. Biochem.* 1994, *115*, 1053–1057.

[50] Turbill, P., Beugeling, T., Poot, A. A., *Biomaterials* 1996, *17*, 1279–1287.

[51] Wu, H., Fan, Y., Sheng, J., Sui, S. F., *Eur. Biophy. J. Biophys. Lett.* 1993, *22*, 201–205.

[52] Silberberg, A., *Surface and Interfacial Aspects of Biomedical Polymers – Protein Adsorption*, Plenum Press, New York 1985.

[53] Wahlgren, M., Arnebrant, T., *Trends Biotechnol.* 1991, *9*, 201–208.

[54] Brash, J., *Proteins at Interfaces – Physiochemical and Biomedical Studies*, American Chemical Society, Washington 1987.

[55] Vorm, O., Roepstorff, P., Mann, M., *Anal. Chem.* 1994, *66*, 3281–3287.

[56] Wei, J., Buriak, J. M., Siuzdak, G., *Nature* 1999, *399*, 243–246.

[57] Thomas, J. J., Shen, Z. X., Crowell, J. E., Finn, M. G., Siuzdak, G., *Proc. Natl. Acad. Sci. USA* 2001, *98*, 4932–4937.

Enhanced Discrimination of Benign from Malignant Prostatic Disease by Selective Measurements of Cleaved Forms of Urokinase Receptor in Serum

Timo Piironen,[1†] Alexander Haese,[2] Hartwig Huland,[2] Thomas Steuber,[2]
Ib Jarle Christensen,[6] Nils Brünner,[3] Keld Danø,[1] Gunilla Høyer-Hansen,[1] and
Hans Lilja[4,5*]

Background: Early detection of prostate cancer (PCa) centers on measurements of prostate-specific antigen (PSA), but current testing practices suffer from lack of specificity and generate many unnecessary prostate biopsies. Soluble urokinase plasminogen activator receptor (uPAR) is present in blood in both intact and cleaved forms. Increased uPAR in blood is correlated with poor prognosis in various cancers, but uPAR has not been shown to be useful in PCa diagnostics. We assessed the ability of immunoassays for specific uPAR forms to discriminate PCa from benign conditions.

Methods: We measured total PSA (tPSA), free PSA (fPSA), intact uPAR [uPAR(I-III)], intact uPAR + cleaved uPAR domains II+III [uPAR(I-III) + uPAR(II-III)], and cleaved uPAR domain I [uPAR(I)] in sera from 224 men with and 166 men without PCa. We assessed differences in serum concentrations between the PCa and noncancer groups within the entire cohort and in men with tPSA concentrations of 2–10 μg/L. The diagnostic accuracy of individual analytes and analyte combinations was explored by logistic regression and ROC analyses and evaluations of sensitivity and specificity pairs.

Results: Serum uPAR(I) and uPAR(II-III) were higher in PCa than in benign disease. In men with tPSA between 2 and 10 μg/L, the combination of %fPSA with the ratio uPAR(I)/uPAR(I-III) had a greater area under the ROC curve (0.73) than did %fPSA (0.68).

Conclusions: Specific measurements of different uPAR forms in serum improve the specificity of PCa detection. The uPAR forms may therefore be complementary to PSA for PCa detection, most importantly in men with moderately increased PSA.

© 2006 American Association for Clinical Chemistry

Prostate-specific antigen (PSA)[7] in serum is used for detection of prostate cancer (PCa), but it is also increased in benign prostatic diseases, which leads to many prostatic biopsies. The proportion of free (unbound) PSA (fPSA) is higher in benign prostatic hyperplasia (BPH) than in PCa. This has led to the use of the ratio of fPSA to total PSA (%fPSA) and improved the specificity for PCa; however, approximately two thirds of patients still undergo unnecessary biopsies.

The major cause of PCa morbidity and mortality is metastatic disease. During the process of tissue remodeling associated with cancer invasion and metastasis, a complex array of proteolytic enzymes participates in matrix degradation (1). The proteases and their regulators can be candidate prognostic or diagnostic tumor markers.

Cell-surface plasminogen activation catalyzed by

urokinase plasminogen activator (uPA) is a major step in the activation of the matrix-degrading protease system in cancer *(2)*. uPA is secreted as an inactive proenzyme, which localizes on the cell surface by binding to a glyco-lipid-anchored cell surface receptor, urokinase plasminogen activator receptor (uPAR). Binding to uPAR enhances the activation of uPA proenzyme because of the proximity of cell-surface–bound plasminogen. uPAR consists of 3 homologous 3-finger domains, of which the amino-terminal domain (I) is required for binding to uPA. However, all domains are needed for high-affinity binding *(3, 4)*. uPA can cleave uPAR in the linker region between domains I and II, liberating domain I [uPAR(I)] and leaving the remainder of the molecule [uPAR(II-III)] on the cell surface *(5)*. In addition, uPAR can be shed from cells by cleavage at the lipid anchor by phospholipases or proteases, liberating full-length uPAR(I-III) and/or uPAR(II-III) *(6, 7)*.

uPAR is expressed in many types of human cancers, often primarily by stromal cells *(1)*. In PCa tissue, uPAR is expressed by macrophages and neutrophils *(8)*. Cleaved uPAR forms are present in several neoplastic cell lines and tissues *(9, 10)*. Increased plasma concentrations of soluble uPAR forms (suPAR) have been found in patients with non–small cell lung cancer *(11)* and colon cancer *(12)*. Furthermore, ovarian cancer cyst fluid contains soluble uPAR(II-III) *(13)*, and urine from patients with acute myeloid leukemia contains uPAR(I) and uPAR(II-III) *(14)*.

Measurements of uPAR forms carry prognostic significance. The concentrations of uPAR in tumor tissue indicate prognosis in squamous cell lung cancer *(15)*, colon cancer *(16)*, and breast cancer *(17)*. In squamous cell lung cancer, uPAR(I) is a stronger prognostic indicator than is total uPAR immunoreactivity *(18)*, and in colorectal cancer *(19)* and breast cancer *(20)*, the concentration of suPAR in blood is significantly associated with prognosis. For PCa, however, measurement of suPAR has not been useful *(21, 22)*. Individual forms of uPAR, however, have not yet been tested for association with PCa. In this study, we assessed the ability of newly developed immunoassays designed for the specific measurement of different suPAR forms *(10)* in serum to discriminate between benign and malignant prostatic disease and compared the performance of theses assays with the performance of %fPSA, free and total PSA.

Materials and Methods

immunoassays

uPAR. Three uPAR immunoassays, TR-FIA 1, TR-FIA 2 and TR-FIA 3, have been designed for the specific measurement of uPAR(I-III), uPAR(I-III) + uPAR(II-III), and uPAR(I), respectively *(10)*. The detection limits were 0.3 pmol/L uPAR(I-III) for TR-FIA 1 and TR-FIA 2 and 1.9 pmol/L uPAR(I) for TR-FIA 3. The assays were previously validated for use in citrate plasma. To validate these assays for use in serum, we made 2 serum pools, using sera from 50 men with total PSA (tPSA) concentrations

ranging from 0.2 to 28.7 μg/L for each pool. We assessed the linearity of the assays by assaying serum diluted (1:2 to 1:128) in assay buffer.

To determine the limit of quantification, we added purified uPAR to uPAR-depleted serum and calculated the CV. To prepare uPAR-depleted serum, we diluted the serum 1:5 in 0.2 mol/L phosphate buffer (pH 7.4) containing 0.1 mol/L NaCl and passed the diluted serum over a protein A–Sepharose CL-4B (Pharmacia Biotech) to adsorb the uPAR. We then passed the eluate from the first column over a protein A–Sepharose column preloaded with a polyclonal rabbit anti-uPAR antibody *(23)* to adsorb the remaining uPAR. The depleted serum contained 7.7% of the initial amounts of uPAR(I-III) measured by TR-FIA 1 and only 4.4% of the initial amounts of uPAR(I-III) + uPAR(II-III) measured by TR-FIA 2. Depletion of uPAR(I) reduced the TR-FIA 3 signal to 14% of that obtained before immunodepletion. We then added purified uPAR(I-III) and uPAR(I) to this depleted serum at concentrations of 0.016–10 μg/L [0.5–325 pmol/L uPAR(I-III) and 1.5–961 pmol/L uPAR(I)]. The limit of quantification was defined as the lowest concentration at which the CV did not exceed 20%.

We assessed the analytical specificities (i.e., immunologic cross-reactivities) of the assays by measuring the concentrations of the uPAR variants in the different assays before and after uPAR depletion of serum. Intra- and interassay precision was determined by measuring 10 or 26 replicates of the serum pool in the 3 TR-FIAs. Because the amount of uPAR(I) in the 1:10-diluted serum pool was close to the limit of quantification, we determined the interassay precision of TR-FIA 3 by adding 480 pmol/L uPAR(I) to serum. All samples were diluted 1:10 in assay buffer before analysis. We determined the recoveries of calibrators added at concentrations of 0.041–8 μg/L [3.9–769 pmol/L uPAR(I) or 1.3–260 pmol/L uPAR(I-III)] in a serum pool diluted (10% by volume) in assay buffer. The recoveries were calculated from the slopes of the lines representing the uPAR(I-III) or uPAR(I) signals as a function of concentration, and 100% recovery was defined as the slope in assay buffer.

We calculated uPAR(II-III) by subtracting the moles of uPAR(I-III) measured in TR-FIA 1 from those of uPAR(I-III) and uPAR(II-III) measured in TR-FIA 2.

tPSA and fPSA. To detect tPSA and fPSA, we used the commercial version of a previously reported dual-label assay (DELFIA® ProStatus™ PSA Free/Total Kit; PerkinElmer Life Sciences) that measures tPSA and fPSA on an equimolar basis. Detection limits were 0.04 μg/L for fPSA (CV = 3.7% at 0.44 μg/L and 18% at 0.10 μg/L) and 0.05 μg/L for tPSA (CV = 5.0% at 2.32 μg/L and 14% at 0.34 μg/L).

samples

We collected 390 consecutive serum samples from patients referred to the Department of Urology at the

University Clinic (UKE) Hamburg, Germany, during 1999–2001. Of these, 367 patients were evaluated for the presence of PCa because of increased tPSA concentrations, suspicious digital rectal examination (DRE), or both. These patients were evaluated by systematic (at least sextant) biopsy of the prostate, which was performed with transrectal ultrasound guidance. Biopsies were taken from the apex, mid region, and base of the left and right peripheral zones. An additional 23 serum samples were taken from patients undergoing transurethral or open surgery for symptomatic BPH in whom pathology work-up of the specimen revealed no evidence of cancer. The median (range) ages were 63 (43–76) years for cancer patients and 64 (47–85) years for noncancer patients. All sera were drawn before any prostatic manipulation. Patients who received 5α-reductase inhibitors for symptomatic relief of BPH were excluded. The collected blood was processed to serum by centrifugation within 2 h; the serum samples were frozen within 6 h, stored at -80 °C, and thawed only immediately before analysis.

STATISTICAL ANALYSES

Descriptive statistics for the measured concentrations of tPSA, fPSA, uPAR(I-III), uPAR(I-III) + uPAR(II-III), and uPAR(I) and the calculated %fPSA and uPAR(II-III) are given as the median (range). Correlation coefficients between these measurements were estimated by rank statistics (Spearman).

Tests for location between the 2 groups of patients were performed with the Mann–Whitney test, with the results obtained by the U-statistic normalized by the total number of combinations (i.e., an estimate of the probability that a randomly selected cancer patient has a higher concentration than a randomly selected non-cancer patient) denoted $P(x>y)$ and its P value.

Results for the total cohort of 390 patients (224 cancer patients and 166 noncancer patients) were analyzed in a blind, randomly organized manner. In addition, a subgroup analysis of those patients with tPSA between 2 and 10 μg/L was subsequently performed.

The probability of cancer for multivariate data was estimated by logistic regression analysis. All entered covariates were log-transformed. Results are presented by the odds ratio (95% confidence interval). Regression diagnostics were evaluated by conventional techniques, and cross-validation was performed (24). Significantly correlated covariates ($r > 0.7$) were not entered simultaneously into the multivariate model.

ROC curves were generated, and the areas under the curves (AUCs) were calculated. Finally, we calculated the specificities for fixed sensitivities of 85%, 90%, and 95% for each covariate and the multivariate result, using a reduced-bias estimate for the predicted probability of an event. Similar estimates of the sensitivity for fixed specificities were calculated. The differences in sensitivity and specificity between models at selected cutpoints were evaluated by McNemar test. In addition, the false-positive (defined as the proportion of incorrectly classified cancers compared with the predicted number of cancers) and false-negative (defined as the proportion of incorrectly classified noncancers compared with the predicted number of noncancers) rates were estimated.

$P < 0.5$ was considered significant. All calculations were done with SAS software (Ver. 9.1; SAS Institute).

Results

VALIDATION OF TR-FIA ASSAYS

The limits of quantification (CV $<20\%$) for uPAR(I-III) were 1.6 pmol/L in TR-FIA 1 and 2.0 pmol/L in TR-FIA 2. For uPAR(I) in TR-FIA 3, the limit of quantification was 1.9 pmol/L. The loss of linearity (defined as a deviation $>20\%$) for TR-FIA 1, TR-FIA 2, and TR-FIA 3 occurred at 1.6, 2.8, and 3.8 pmol/L, respectively.

Intraassay imprecision (CV; Table 1) was $<20\%$ in all cases except for TR-FIA 3 in serum diluted 1:10, in which the uPAR(I) concentration was at the limit of quantification. We nonetheless used this dilution routinely because only limited sample volumes were available. Interassay imprecision results are given in Table 1.

The recoveries in TR-FIA 2 and TR-FIA 3 were 89% and 99%, respectively. The recovery of uPAR(I-III) in 10% serum (in buffer) measured by TR-FIA 1 was only 75%. This may reflect that the serum pool contains uPA or another uPAR ligand that binds uPAR and thus prevents full recovery of the added uPAR(I-III).

FINDINGS IN ENTIRE COHORT

For the entire cohort of 390 patients, median (range) tPSA was 6.99 (0.27–87.1) μg/L. The median tPSA concentrations were 7.82 μg/L in patients with histologically confirmed PCa (n = 224) vs 5.58 μg/L in patients with no evidence of PCa (n = 166). The concentrations of uPAR(I-III) and uPAR(I-III) + uPAR(II-III) in all 390 samples were above the limits of quantification for the TR-FIA 1 and TR-FIA 2 assays, whereas in 6 of the 390 samples, the uPAR(I) concentrations were below the limit of quantifi-

Table 1. Intra- and interassay precision of uPAR immunoassays, based on measurements in 10% serum (in assay buffer).

Assay	Intraassay				Interassay			
	Mean, pmol/L	SD, pmol/L	CV, %	n	Mean, pmol/L	SD, pmol/L	CV, %	n
TR-FIA 1	41	2.9	7.0	26	55	10.4	19	10
TR-FIA 2	114	5.9	5.2	26	139	16.4	12	10
TR-FIA 3	37	12.5	35	26	409[a]	59.0[a]	14[a]	10

[a] Measured in samples to which 480 pmol/L uPAR(I) had been added.

cation for TR-FIA 3. Descriptive statistics for all measurements and the results of the Mann–Whitney test for location, including the statistical measure for discrimination $P(x>y)$, are shown in Table 2A.

uPAR(I-III) and uPAR(I-III) + uPAR(II-III) were highly correlated, whereas all uPAR measurements were weakly correlated with tPSA, fPSA, and %fPSA (Table 3). The Spearman correlation coefficients for patients, stratified by cancer/noncancer, showed similar results in each stratum (data not shown).

Multivariate analysis (Table 4A) of the above measurements included tPSA, %fPSA, uPAR(I-III), and uPAR(I), but uPAR(I-III)+uPAR(II-III) was not included because it was highly correlated with uPAR(I-III). Including age in the multivariate model did not alter the results ($P = 0.19$, dichotomized by the median). uPAR(I-III) was not significant in the univariate model, whereas it was significant in the multivariate model including uPAR(I), suggesting an interrelationship between these covariates. The regression coefficients for uPAR(I) and uPAR(I-III) were similar in magnitude. The negative character of uPAR(I-III) implies that the model could be formulated as the ratio of uPAR(I) to uPAR(I-III). The χ^2 value for model 2 was 69.06 (compared with 69.52 for model 1), suggesting that the ratio of uPAR(I) to uPAR(I-III) adequately describes the data illustrated in Table 4A.

PATIENTS WITH tPSA BETWEEN 2 AND 10 μg/L

Among 255 men with moderately increased tPSA (between 2 and 10 μg/L), median tPSA concentrations were 6.31 μg/L in 139 patients with PCa vs 5.14 μg/L in 116 patients with no evidence of malignancy. The results of multivariate analysis in this subgroup are shown in Table 4B, where the ratio uPAR(I)/uPAR(I-III) is included (tPSA is not a statistically significant prognostic variable in the model).

ROC ANALYSIS

To assess the accuracy of the multivariate models incorporating different combinations of variables, we calculated AUCs for the ROC curves (Fig. 1). For the entire set of patients, the AUC of tPSA alone was 0.65 [95% confidence interval (CI), 0.60–0.70]. For a model combining tPSA and %fPSA, the AUC was 0.75 (0.70–0.80), which further increased to 0.78 (0.74–0.82) for the combination of tPSA, %fPSA, and the ratio uPAR(I)/uPAR(I-III). This further increase was statistically highly significant ($P <0.001$).

In the entire tPSA range, specificities for tPSA were 15%, 24%, and 32% at sensitivities of 95%, 90%, and 85%, respectively. From this baseline, specificity increased by 10% to 19% when we used the calculated combinations of tPSA, fPSA, and the tested uPAR forms (Table 5A). The widths of the 95% CIs for the shown sensitivities ranged from 9% to 13% and from 10% to 15% for the specificities.

Table 2. Descriptive statistics for PCa vs noncancer.

A. All patients

Covariate	Median (range)[a] PCa	Median (range)[a] Negative	$P(x>y)$	P
tPSA, μg/L	7.82 (0.27–87.10)	5.58 (0.65–39.80)	0.65	<0.001
fPSA, μg/L	0.95 (0.06–4.20)	0.95 (0.13–15.20)	0.52	0.73
%fPSA[b]	11.92 (4.31–44.28)	19.72 (3.20–71.70)	0.74	<0.001
uPAR(I-III), pmol/L	48.93 (23.93–85.94)	49.38 (26.49–125.63)	0.54	0.22
uPAR(I-III) + uPAR(II-III), pmol/L	98.54 (47.94–164.79)	94.27 (39.17–280.49)	0.54	0.15
uPAR(I), pmol/L	72.04 (10.38–256.34)[c]	61.48 (5.26–193.10)[c]	0.60	0.001
uPAR(II-III),[b] pmol/L	48.30 (14.97–100.72)	44.27 (12.67–154.87)	0.60	0.0006
uPAR(I)/uPAR(I-III)[b]	1.48 (0.26–4.91)	1.16 (0.12–2.99)	0.64	<0.001

B. Patients with tPSA between 2 and 10 μg/L

Covariate	Median (range)[a] PCa	Median (range)[a] Negative	$P(x>y)$	P
tPSA, μg/L	6.31 (2.05–9.87)	5.14 (2.10–9.97)		
fPSA, μg/L	0.78 (0.29–3.56)	0.91 (0.19–3.31)	0.56	0.09
%fPSA[b]	13.25 (4.31–44.28)	19.03 (3.20–53.26)	0.68	<0.001
uPAR(I-III), pmol/L	49.94 (23.93–83.16)	49.03 (26.49–125.63)	0.54	0.22
uPAR(I-III) + uPAR(II-III), pmol/L	97.93 (51.03–160.52)	91.87 (39.17–280.49)	0.52	0.48
uPAR(I), pmol/L	69.35 (14.61–256.34)[d]	58.90 (7.60–193.10)[e]	0.59	0.014
uPAR(II-III),[b] pmol/L	47.39 (20.13–100.72)	43.59 (12.67–154.87)	0.59	0.019
PAR(I)/uPAR(I-III)[b]	1.44 (0.33–4.91)	1.17 (0.19–2.65)	0.63	0.0004

[a] No. of men in groups: n = 224 for all patients with PCa; n = 166 for all noncancer patients; n = 139 for PCa patients with tPSA between 2 and 10 μg/L; and n = 116 for noncancer patients with tPSA between 2 and 10 μg/L.

[b] Calculated.

[c] In this group, 3 samples had uPAR(I) concentrations below the limit of quantification for TR-FIA 3.

[d] In this group, 1 sample had uPAR(I) concentrations below the limit of quantification for TR-FIA 3.

[e] In this group, 2 samples had uPAR(I) concentrations below the limit of quantification for TR-FIA 3.

Table 3. Rank correlation coefficients and *P* values, all patients (n = 390).

	fPSA	%fPSA[a]	uPAR(I-III)	uPAR(I-III) + uPAR(II-III)	uPAR(I)	uPAR(II-III)[a]	uPAR(I)/uPAR(I-III)[a]
tPSA							
r	0.73	−0.40	0.01	0.06	0.05	0.10	0.06
P	<0.001	<0.001	0.77	0.20	0.34	0.05	0.27
fPSA							
r		0.26	0.07	0.12	0.09	0.12	0.06
P		<0.001	0.17	0.02	0.07	0.02	0.21
%fPSA[a]							
r			0.07	0.06	0.01	0.02	−0.04
P			0.16	0.26	0.89	0.69	0.41
uPAR(I-III)							
r				0.82	0.44	0.46	−0.01
P				<0.001	<0.001	<0.001	0.84
uPAR(I-III) + uPAR(II-III)							
r					0.54	0.87	0.19
P					<0.001	<0.001	<0.001
uPAR(I)							
r						0.49	0.88
P						<0.001	<0.001
uPAR(II-III)[a]							
r							0.31
P							<0.001

[a] Calculated.

For 90% sensitivity, the false-positive rate was 41% for tPSA, which decreased to 32% in the multivariate model. Similarly, the false-negative rate decreased from 46% to 24%.

For patients with tPSA of 2–10 μg/L (Fig. 1B), the AUCs for %fPSA and for the combination of %fPSA with the ratio uPAR(I)/uPAR(I-III) were 0.68 (95% CI, 0.62–0.79) and 0.73 (0.67–0.79) (P <0.001). In this group, specificities for %fPSA were 10%, 19%, and 36% at sensitivities of 95%, 90%, and 85%, respectively. Specificity increased up to

Table 4. Logistic regression analysis (multivariate analysis) to predict cancer on biopsy.

A. All patients (n = 390)

	P	Odds ration	95% CI
Model 1			
Log tPSA	0.034	1.43	1.03–2.00
Log %fPSA	<0.001	0.16	0.09–0.28
Log uPAR(I)	<0.001	3.12	1.91–5.09
Log uPAR(I-III)	0.002	0.19	0.07–0.55
Model 2			
Log tPSA	0.035	1.43	1.03–1.99
Log %fPSA	<0.001	0.16	0.09–0.27
Log uPAR(I)/uPAR(I-III)	<0.001	3.11	1.90–5.07

B. Patients with tPSA between 2 and 10 μg/L (n = 255)

Model 1			
Log %fPSA	<0.001	0.22	0.12–0.42
Log uPAR(I)	<0.001	3.22	1.84–5.61
Log uPAR(I-III)	0.002	0.13	0.04–0.47
Model 2			
Log %fPSA	<0.001	0.22	0.12–0.41
Log uPAR(I)/uPAR(I-III)	<0.001	3.15	1.81–5.47

41% when we used the calculated combinations of %fPSA and the tested uPAR forms (Table 5B). The widths of the 95% CIs for the shown sensitivities ranged from 8% to 13% and from 10% to 15% for the specificities. For 90% sensitivity, the false-positive rate was 43% for %fPSA, which decreased to 41% for the multivariate model, whereas the false-negative rate was decreased from 39% to 31%. The tests for differences in sensitivities and specificities at the chosen cutpoints are descriptive and should not be interpreted as confirmative tests. This can also be seen in Fig. 1, in which differences are even greater in the middle range. Moreover, false-positive and -negative rates are dependent on the study population and would differ in a population with another cancer prevalence.

Discussion

The results of this study indicate that uPAR forms can improve discrimination of PCa from nonmalignant sources of increased PSA and that tPSA and fPSA correlate only weakly with the concentrations of uPAR forms (Table 3). Thus, uPAR forms are largely independent analytical variables, conceivably offering clinical information that is different from and additive to that contributed by fPSA and tPSA. Various mechanisms have been proposed for the release of soluble forms of uPAR in the serum, including cleavage at the lipid anchor by phospholipases and proteases to release full-length and cleaved receptor, cleavage and release of domain I by uPA or other proteases, or a combination of these events. Furthermore, it is possible that the amounts of uPAR(I) and uPAR(II-III) in the circulation may be directly related to the extent of uPA-catalyzed plasminogen activation and
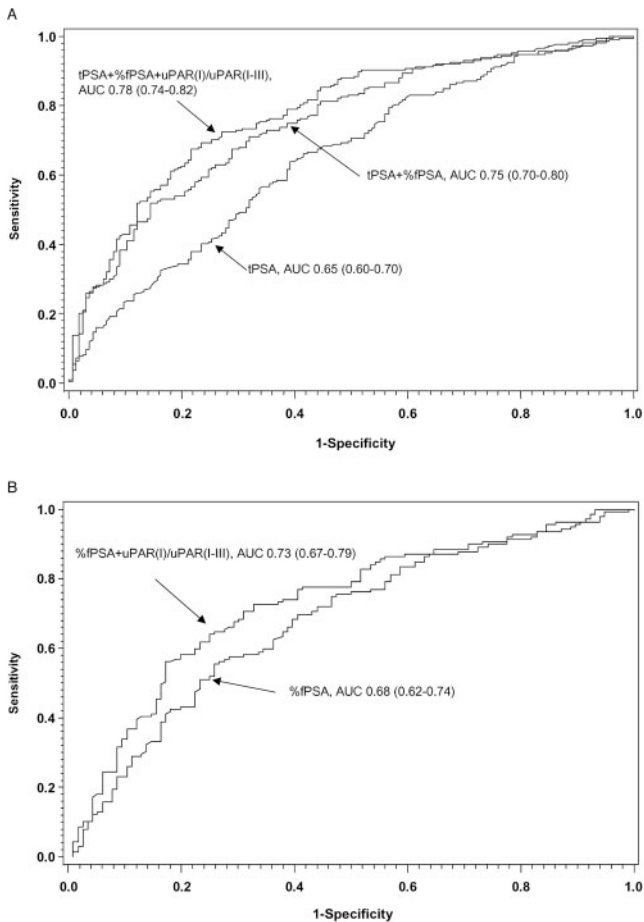
Fig. 1. ROC analysis and AUC (95% CI) calculated for PSA forms for the entire cohort (*A*) and for men with tPSA between 2 and 10 μg/L (*B*).

(*A*), ROC curves for tPSA, tPSA + %fPSA, and tPSA + %fPSA + uPAR(I)/uPAR(I-III) for the entire study cohort (n = 390). (B), ROC curves for %fPSA and %fPSA + uPAR(I)/uPAR(I-III) for men with tPSA between 2 and 10 μg/L (n = 255).

factor in measurements of uPAR because the increased amount of uPA observed in men with PCa (*21, 25*) may cause uPAR(I-III) concentrations to be underestimated in sera collected from these men. Among the measured 390 samples, all were above the limits of quantification for the TR-FIA 1 and TR-FIA 2 assays, and only 6 were below the experimentally determined limit of quantification for TR-FIA 3. Analysis of the diagnostic utility of the combination of uPAR forms with PSA forms can be accomplished by logistic regression analysis. Logistic regression analyses using combinations of variables frequently provide better discrimination than simple algorithms, e.g., ratios calculated from the individual measurements from each patient. Logistic regression analysis is instrumental in providing the basis for various risk analysis systems that support medical decision-making.

The optimal cutoff concentration depends on whether high sensitivity or high specificity is preferred in detecting PCa. In this consecutive cohort of referral patients, men were either symptomatic for BPH or had been recommended for prostate biopsy because of previous findings of increased tPSA and/or abnormal DRE results. ROC analyses revealed significant clinical information from 2 of the 3 uPAR immunoassays, which measure uPAR(I-III) and uPAR(I).

The discriminative power of the uPAR forms as individual analytes is not as powerful as that of tPSA or %fPSA. In the unrestricted PSA group and in both groups, tPSA and %fPSA, respectively, discriminated highly significantly between biopsy outcomes. In contrast, only the directly measured uPAR(I) and the calculated uPAR(I)/uPAR(I-III) were significant discriminators. These improvements were achieved not only in relation to tPSA alone, but also in relation to the more recently introduced use of %fPSA.

The most clinically relevant application of uPAR measurements, as evidenced in our study, is the tPSA range <10 μg/L. In this clinical scenario, the use of an algorithm that combines fPSA with uPAR would increase the AUC from 67% to 73%. It is in this tPSA range that the need for

thus may be stronger diagnostic/prognostic markers than the total amount of uPAR. Increased concentrations of uPA in sera from PCa patients may be a confounding

Table 5. ROC analysis: Specificities and sensitivities in discriminating prostate cancer vs noncancer.

A. All patients (n = 390)

Variables in model	Specificity (%) at sensitivity of			Sensitivity (%) at specificity of		
	85%	90%	95%	85%	90%	95%
tPSA	32	24	15	27	22	13
tPSA + %fPSA	44	37	14	51	37	27
uPAR(I)	22	16	8	22	15	10
tPSA + %fPSA + uPAR(I) + uPAR(I-III)	51[a]	39	25[a]	52	44[a]	26
tPSA + %fPSA + uPAR(I)/uPAR(I-III)	51[a]	43[a]	22[a]	55	44[a]	30

B. Patients with tPSA between 2 and 10 μg/L (n = 255)

Variables in model	Specificity (%) at sensitivity of			Sensitivity (%) at specificity of		
%fPSA	19	36	10	30	22	11
uPAR(I)	16	26	4	21	16	11
%fPSA + uPAR(I) + uPAR(I-III)	29[b]	41	16[b]	49[b]	29	17[c]
%fPSA + uPAR(I)/uPAR(I-III)	27[b]	41	13	43[b]	31[c]	22[b]

[a] *P* <0.05 compared with tPSA + %fPSA.
[b,c] Compared with %fPSA: [b] *P* <0.05; [c] *P* <0.10.

additional biomarkers is greatest because of the favorable outcome when PCa is detected early on the one hand, and the relatively high number of patients without cancer who might be spared an invasive, potentially harmful, and costly prostate biopsy on the other hand.

References

1. Danø K, Behrendt N, Høyer-Hansen G, Johnsen M, Lund LR, Ploug M, et al. Plasminogen activation and cancer. Thromb Haemost 2005;93:676–81.
2. Almholt K, Lund LR, Rygaard J, Nielsen BS, Danø K, Rømer J, et al. Reduced metastasis of transgenic mammary cancer in urokinase-deficient mice. Int J Cancer 2005;113:525–32.
3. Ploug M. Structure-function relationships in the interaction between the urokinase-type plasminogen activator and its receptor. Curr Pharm Des 2003;9:1499–528.
4. Llinas P, Le Du MH, Gardsvoll H, Danø K, Ploug M, Gilquin B, et al. Crystal structure of the human urokinase plasminogen activator receptor bound to an antagonist peptide. EMBO J 2005;24:1655–63.
5. Høyer-Hansen G, Rønne E, Solberg H, Behrendt N, Ploug M, Lund LR, et al. Urokinase plasminogen activator cleaves its cell surface receptor releasing the ligand-binding domain. J Biol Chem 1992;267:18224–9.
6. Wilhelm OG, Wilhelm S, Escott GM, Lutz V, Magdolen V, Schmitt M, et al. Cellular glycosylphosphatidylinositol-specific phospholipase D regulates urokinase receptor shedding and cell surface expression. J Cell Physiol 1999;180:225–35.
7. Beaufort N, Leduc D, Rousselle JC, Magdolen V, Luther T, Namane A, et al. Proteolytic regulation of the urokinase receptor/CD87 on monocytic cells by neutrophil elastase and cathepsin G. J Immunol 2004;172:540–9.
8. Usher PA, Thomsen OF, Iversen P, Johnsen M, Brünner N, Høyer-Hansen G, et al. Expression of urokinase plasminogen activator, its receptor and type-1 inhibitor in malignant and benign prostate tissue. Int J Cancer 2005;113:870–80.
9. Solberg H, Rømer J, Brünner N, Holm A, Sidenius N, Danø K, et al. A cleaved form of the receptor for urokinase-type plasminogen activator in invasive transplanted human and murine tumors. Int J Cancer 1994;58:877–81.
10. Piironen T, Laursen B, Pass J, List K, Gårdsvoll H, Ploug M, et al. Specific immunoassays for detection of intact and cleaved forms of the urokinase receptor. Clin Chem 2004;50:2059–68.
11. Pappot H, Høyer-Hansen G, Rønne E, Hansen HH, Brünner N, Danø K, et al. Elevated plasma levels of urokinase plasminogen activator receptor in non-small cell lung cancer patients. Eur J Cancer 1997;33:867–72.
12. Stephens RW, Pedersen AN, Nielsen HJ, Hamers MJ, Høyer-Hansen G, Rønne E, et al. ELISA determination of soluble urokinase receptor in blood from healthy donors and cancer patients. Clin Chem 1997;43:1868–76.
13. Wahlberg K, Høyer-Hansen G, Casslen B. Soluble receptor for urokinase plasminogen activator in both full-length and a cleaved form is present in high concentration in cystic fluid from ovarian cancer. Cancer Res 1998;58:3294–8.
14. Mustjoki S, Sidenius N, Sier CF, Blasi F, Elonen E, Alitalo R, et al. Soluble urokinase receptor levels correlate with number of circulating tumor cells in acute myeloid leukemia and decrease rapidly during chemotherapy. Cancer Res 2000;60:7126–32.
15. Pedersen H, Brünner N, Francis D, Osterlind K, Rønne E, Hansen HH, et al. Prognostic impact of urokinase, urokinase receptor, and type 1 plasminogen activator inhibitor in squamous and large cell lung cancer tissue. Cancer Res 1994;54:4671–5.
16. Ganesh S, Sier CF, Heerding MM, Griffioen G, Lamers CB, Verspaget HW. Urokinase receptor and colorectal cancer survival. Lancet 1994;344:401–2.
17. Grøndahl-Hansen J, Peters HA, van Putten WL, Look MP, Pappot H, Rønne E, et al. Prognostic significance of the receptor for urokinase plasminogen activator in breast cancer. Clin Cancer Res 1995;1:1079–87.
18. Almasi CE, Høyer-Hansen G, Christensen IJ, Danø K, Pappot H. Prognostic impact of liberated domain I of the urokinase plasminogen activator receptor in squamous cell lung cancer tissue. Lung Cancer 2005;48:349–55.
19. Stephens RW, Nielsen HJ, Christensen IJ, Thorlacius-Ussing O, Sorensen S, Danø K, et al. Plasma urokinase receptor levels in patients with colorectal cancer: relationship to prognosis. J Natl Cancer Inst 1999;91:869–74.
20. Riisbro R, Christensen IJ, Piironen T, Greenall M, Larsen B, Stephens RW, et al. Prognostic significance of soluble urokinase plasminogen activator receptor in serum and cytosol of tumor tissue from patients with primary breast cancer. Clin Cancer Res 2002;8:1132–41.
21. Miyake H, Hara I, Yamanaka K, Gohji K, Arakawa S, Kamidono S. Elevation of serum levels of urokinase-type plasminogen activator and its receptor is associated with disease progression and prognosis in patients with prostate cancer. Prostate 1999;39:123–9.
22. McCabe NP, Angwafo FF 3rd, Zaher A, Selman SH, Kouinche A, Jankun J. Expression of soluble urokinase plasminogen activator receptor may be related to outcome in prostate cancer patients. Oncol Rep 2000;7:879–82.
23. Rønne E, Høyer-Hansen G, Brünner N, Pedersen H, Rank F, Osborne CK, et al. Urokinase receptor in breast cancer tissue extracts. Enzyme-linked immuno-sorbent assay with a combination of mono- and polyclonal antibodies. Breast Cancer Res Treat 1995;33:199–207.
24. Harrell FE, Lee KL, Mark DB. Multivariable prognostic models: issues in developing models, evaluating assumptions and adequacy, and measuring and reducing errors. Stat Med 1996;15:361–87.
25. Wun TC, Schleuning WD, Reich E. Isolation and characterization of urokinase from human plasma. J Biol Chem 1982;257:3276–83.

Comparison of free and total forms of serum human kallikrein 2 and prostate-specific antigen for prediction of locally advanced and recurrent prostate cancer

Thomas Steuber,[1,2] Andrew J. Vickers,[1,3] Angel Serio,[1] Ville Vaisanen,[4] Alexander Haese,[2] Kim Pettersson,[4] James A. Eastham,[1] Peter T. Scardino,[1] Hartwig Huland,[2] and Hans Lilja[1,5,6]

[1] Department of Urology, Memorial Sloan-Kettering Cancer Center, New York, USA

[2] Department of Urology, University Hospital Hamburg-Eppendorf, Hamburg, Germany

[3] Department of Epidemiology and Biostatistics, Memorial Sloan-Kettering Cancer Center, New York, USA

[4] Department of Biotechnology, University of Turku, Turku, Finland

[5] Department of Clinical Laboratories, Urology and Medicine, Memorial Sloan-Kettering Cancer Center, New York, USA

[6] Department of Laboratory Medicine, Division of Clinical Chemistry, Lund University, University Hospital (UMAS), Malmö, Sweden

Address all correspondence to:
Thomas Steuber, M.D.
Department of Urology
University Hospital Hamburg-Eppendorf
Hamburg, Germany
steuber@uke.uni-hamburg.de
Phone: (040) 42803 – 3443
Fax: (040) 42803 - 6837

Conflict of interest: In full disclosure of potential conflicts of interest, we would like to notify that Dr. Hans Lilja is a patent holder of free PSA and hK2 immunoassays. The authors affirm that no further relationships exist that could be construed as resulting in an actual, potential or apparent conflict of interest with the manuscript submitted for review.

Running title: hK2 and PSA in prostate cancer prediction
Key words: prostate cancer, prostate-specific antigen, human kallikrein 2, cancer recurrence

Abstract

Introduction: We evaluated the association of total and free forms of serum human kallikrein 2 (hK2) and prostate-specific antigen (PSA) with prostate cancers of unfavorable prognosis.

Methods: We retrospectively measured total PSA (tPSA), free PSA (fPSA), total hK2 (thK2), and free hK2 (fhK2) in pre-operative serum samples from 867 men treated with radical prostatectomy for clinically localized prostate cancer. Associations between biomarker levels and extracapsular extension, seminal vesicle invasion, and biochemical recurrence (BCR) were evaluated. A subset analysis was performed using patients with PSA ≤10 ng/ml, the group most commonly seen in clinical practice in the US.

Results: ThK2 was the strongest predictor of extracapsular extension and seminal vesicle invasion (area under receiver operating characteristic curve [AUC] 0.662 and 0.719, respectively), followed by tPSA (AUC 0.654, 0.663). All biomarkers were significant predictors of BCR. HK2 forms, but not PSA forms, retained important predictive value in the low PSA group. For these men, thK2 was significantly superior to tPSA for predicting BCR (concordance index 0.739 for thK2 vs. 0.566 for tPSA, p<0.0005). Combining tPSA, fPSA, and thK2 in a multivariable model improved prediction compared with any biomarker used individually (AUC 0.714, 0.762, and 0.763 for the prediction of extracapsular extension, seminal vesicle invasion, and BCR, respectively).

Conclusion: Elevated hK2 forms are more strongly associated with advanced prostate cancer than free or total PSA. HK2 retains the ability to discriminate locally advanced and recurrent cancer in patients with PSA ≤10 ng/ml. The incorporation of hK2 into risk-prediction models should be considered.

Introduction

Prostate-specific antigen (PSA; hK3 protein) is the protein product of the human *KLK3* gene. Because of its remarkable tissue specificity in human males, PSA represents the most valuable biomarker for prostate cancer (PCa) identified so far. Besides its established clinical application for early detection, PSA represents a key variable in current prognostic models for clinically localized PCa ([1-3]). These models allow us to assess pathologic tumor stage and the risk of disease recurrence after local therapy; however, PSA levels in blood do not solely reflect the presence of cancer. They are also driven by nodular hyperplastic or inflammatory processes. This limits the application of PSA as a predictor of stage and disease progression in populations in which PSA is regularly used for screening ([4-6]).

Human kallikrein 2 (hK2), the product of the *KLK2* gene, is a serine protease with 80% sequence identity to PSA. The enzymes share the property of being expressed chiefly in the prostate under androgen regulation ([7]).

Various tissue studies have documented increases in the ratio of hK2 expression vs. PSA expression during carcinogenesis and PCa progression ([8-10]). Thus, it was hypothesized that hK2 might be a useful biomarker for PCa, and for advanced disease in particular. It is, however, unclear whether protein levels in tissue correlate with those in circulation; PSA and hK2 levels are up to 10^6-fold higher in tissue compared with blood ([11]). Nevertheless, recent studies have demonstrated that hK2 levels in serum are significantly associated with extracapsular extension (ECE) and with the volume of PCa in prostatectomy specimens ([12-14]). Although these studies have provided indications that serum hK2 may be a predictor of advanced prostate cancer, as yet we lack definitive evidence.

To compare prostate-specific kallikreins in blood for the discrimination of favorable from unfavorable PCa, we assessed free and total PSA, total hK2 (thK2), and free hK2 (fhK2) in a large contemporary series of 867 patients treated with RP for clinically localized PCa. Pre-treatment levels of biomarkers were tested for the capacity to reflect the presence of ECE or seminal vesicle invasion (SVI). Both ECE and SVI are commonly accepted as adverse prognostic factors (15-17). Biochemical recurrence (BCR) following RP represents an unequivocal indicator of eventual clinical progression (18) and was, thus, chosen as a further study endpoint. This represents the first clinical evaluation that includes selective measurements of fhK2.

Materials and Methods

Patients and serum samples

Between January 1997 and September 2004, 1340 patients with clinically localized PCa underwent RP at a single institution (University Hospital Hamburg-Eppendorf, Germany). For 905 of these patients, a pre-treatment serum sample was available for evaluation. Pre-treatment blood samples were drawn eight or more weeks after any prostatic manipulation. Samples were immediately processed and frozen at -80° C until analysis. Patients with any neoadjuvant therapy (n=18) or prior surgical treatment for benign prostate hyperplasia (n=20) were omitted from this study, leaving 867 patients with corresponding blood samples eligible for analysis.

All patients treated with RP were scheduled for an annual follow-up visit at our institutional outpatient clinic. Among the 867 patients, 784 patients had at least one follow-up evaluation, and hence were eligible for analysis of BCR. Informed consent was obtained from all of the participating patients, and the protocol was approved by the institutional review board.

Pathologic evaluation

All RP specimens were surface-inked and processed using serial transverse sections at 3-mm intervals according to the Stanford protocol ([19]). Pathologic stage was defined according to the 1997 AJCC staging classification ([20]). Tumors infiltrating the seminal vesicles were defined as SVI. Our definition of ECE included cancers with or without SVI.

Definition of biochemical recurrence

BCR was defined as postoperative levels of total PSA (tPSA) $\geq$ 0.40 ng/ml. The selection of this cut point was based on a study that demonstrated that a significant proportion of patients with a lower PSA (e.g., 0.2 ng/ml or 0.3 ng/ml) did not experience further PSA rises ([21]). None of the patients received adjuvant therapy prior to evidence of cancer recurrence.

Measurements of biomarkers

Total and free PSA: To measure tPSA and free PSA (fPSA), we used the commercial version of a previously reported dual-label assay (DELFIA Prostatus Dual Assay, Perkin Elmer, Turku, Finland) that measures tPSA and fPSA on an equimolar basis ([22]). Detection limits were 0.04 ng/ml for fPSA (coefficient of variation [CV] 3.7% at 0.44 ng/ml and 17.9% at 0.10 ng/ml), and 0.05 ng/ml for tPSA (CV 5.0% at 2.32 ng/ml and 13.9% at 0.34 ng/ml). The percentage of free PSA (%fPSA) was calculated as %fPSA= fPSA/tPSA*100.

Total and free hK2: PSA- and hK2-specific monoclonal antibodies were used in solid-phase, two-site immunofluorometric assays to detect free and total hK2 ([23]). The total hK2 assay used PSA-specific antibodies to block non-specific signals. The capture antibody of the free hK2

assay did not cross-react with PSA. The functional detection limit (defined as the concentration at which the intra-assay CV was <15%) in serum was 0.003 ng/ml for thK2 and 0.01 ng/ml for fhK2. The thK2 assay imprecision ranged from 2.8% for low (0.01 ng/ml) to 1.6% for high (4.28 ng/ml) hK2 levels. Assay imprecision for fhK2 detection ranged from 3.7% for low (0.01 ng/ml) to 2.0% for high (3.34 ng/ml) hK2 concentrations. In 111 of the 905 patients whose serum was analyzed, the measured proportion of fhK2 to thK2 was 120% or higher because of a previously reported problem with non-specific interactions with serum components ([23](#)); these measurements were excluded from the analysis. For an additional 203 of the 905 patients, we lacked sufficient sample to measure fhK2. In total, levels of fhK2 are not reported for 290 patients of the 867 who were eligible for final analysis.

Statistical methods

To facilitate comparisons between biomarkers in univariate and multivariable analyses, we standardized each marker by dividing by its standard deviation (SD) within the group under consideration. The coefficient in the regressions can thus be interpreted as the change in log odds/hazard for a one standard deviation increase in the predictor. Analyses were performed using Stata 8.2 (Stata Corp., College Station, TX) and S-PLUS software with the Design library (Version 6.2, Insightful Corp.).

Risk assessment for ECE and SVI: Univariate logistic regression analysis was performed to assess the association of all biomarkers with the presence of ECE or SVI. Diagnostic accuracy of each variable was quantified by the area under the receiver operating characteristic (ROC) curve (AUC), which ranges from 0.5 (chance or a coin flip) to 1.0 (perfect ability to rank).

Multivariable regression models were generated to assess whether prediction would be improved by combining markers; the AUC was adjusted by bootstrap methods (24).

Risk assessment for biochemical recurrence: Cox proportional hazards regression was used to determine the association between each biomarker and BCR after RP. We constructed multivariable models including a combination of all biomarkers, again using bootstrap methods to correct for overfit. Predictive accuracy was defined in terms of the concordance index (c-index). In brief, the c-index is a generalization of the area under the ROC curve for survival time data, and quantifies discrimination for a single-variable or a multivariable model.

Comparison of predictive accuracy: We sought to determine whether a single biomarker or combination of biomarkers enhanced predictive accuracy compared with tPSA alone. We used the tPSA alone as the comparator, since tPSA is the marker most frequently used for prediction of ECE, SVI, and BCR. Significance tests for differences in AUC and c-index were conducted, respectively, using the *roccomp* command in Stata and the *rcorrp.cens* function from the Design library of S-PLUS.

Free hK2 measurements were available for only 577 patients. Consequently, fhK2 and %fhK2 were evaluated separately. This cohort, however, did not differ significantly with regard to their clinical and pathological characteristics from the whole cohort of 867 patients. For the sake of simplicity, the fhK2 and %fhK2 results are displayed in the same tables as analysis of thK2, tPSA and fPSA for all 867 patients is presented. For comparison of predictive accuracy, the comparator for fhK2 and %fhK2 was the AUC/c-index calculated for tPSA excluding patients for whom fhK2 was missing.

A subgroup analysis was performed on men with moderately elevated tPSA levels (≤ 10 ng/ml), who are more typical of PCa patients in the US and other countries where tumors are generally detected by PSA screening.

Results

Clinical and pathologic characteristics of the study population are displayed in Table 1. This cohort is reasonably representative of a contemporary referral population (25). ECE or SVI was observed in 249 (29%) and 87 (10%) patients, respectively. In sub-analysis of the 627 men with pre-treatment PSA ≤ 10 ng/ml, ECE or SVI was present in 142 (23%) and 43 (7%) patients, respectively. Median concentrations of tPSA, fPSA, thK2, and fhK2 increased with increasingly adverse prostate pathology: concentrations were lowest in the overall cohort and highest in patients with SVI (Table 2). Conversely, %fPSA and %fK2 decreased with increasingly adverse pathology (Table 2).

Prediction of ECE and SVI: The associations of biomarkers with ECE and SVI are shown in Tables 3 and 4. Total hK2 was the strongest discriminator of ECE from non-ECE. However, compared with tPSA alone, thK2 alone was not a significantly superior classifier of ECE, either in the entire cohort (AUC=0.654 for tPSA and AUC=0.662 for thK2; p=0.6; Table 3) or in the low PSA subgroup (AUC=0.584 and AUC=0.625, respectively; p=0.19; Table 4). Combining tPSA, fPSA and thK2 into a single multivariable model significantly enhanced discrimination of ECE compared with the use of tPSA alone for both the whole sample and the low PSA subgroup (p=0.001 and p=0.01, respectively). This model, however, was not enhanced by adding fhK2 or any ratio of single markers (data not shown).

The strongest predictor of SVI was thK2 (Tables 3 and 4). Total hK2 alone was not a significantly superior classifier of SVI compared with tPSA alone in the whole sample (AUC=0.719 and AUC=0.663, respectively; p=0.09). In the low PSA subgroup, however, the predictive accuracy of thK2 alone was significantly greater than that of tPSA alone (AUC=0.662 and AUC=0.542, respectively; p=0.03). Moreover, the decrease in predictive accuracy from the whole sample to the low PSA subgroup was much larger for tPSA (0.121) than for thK2 (0.057). These results suggest that thK2 is a stronger predictor of SVI compared with tPSA in the low PSA subgroup. Although fhK2 alone and %fhK2 alone had higher AUCs compared with tPSA alone in the low PSA subgroup, these differences were not statistically significant (p=0.14 and p=0.5, respectively). As was the case with ECE, combining tPSA, fPSA, and thK2, but not fhK2, into a single multivariable model significantly enhanced predictive accuracy compared with the use of tPSA alone for both the entire sample (p=0.0005) and the low PSA subgroup (p=0.002).

Prediction of biochemical recurrence: Median follow-up for patients without BCR was 36 months. Among 784 patients eligible for analysis of BCR, there were 119 cases of BCR. The 3- and 5-year recurrence-free probabilities for the study cohort were 83% (95% confidence interval [CI], 80% to 86%) and 74% (95% CI, 68% to 79%), respectively. Forty-seven patients with tPSA $\leq$ 10 ng/ml (n= 556) experienced BCR. The 3- and 5-year recurrence-free probabilities for those men were 91% (95% CI, 87% to 93%) and 84% (95% CI, 77% to 88%), respectively.

Associations between biomarkers and BCR are displayed in Table 5. HK2 forms were the strongest predictors of BCR. This was particularly marked in the low PSA group, where the predictive accuracy of the hK2 forms was significantly greater than that of tPSA alone (c-index 0.739 and 0.758 for total and fhK2, respectively, vs. 0.566 for tPSA; both p<0.0005). The c-

index for fhK2 is apparently larger than that of total hK2; however, this is an unfair comparison, since the fhK2 analysis is based on a subgroup. As a sensitivity analysis, we calculated the c-index for thK2 in the low PSA subgroup, excluding patients where fhK2 was missing; the c-index for thK2 among these patients was 0.775, which was higher than that of fhK2. Combining tPSA, fPSA and thK2 into a single multivariable model significantly enhanced predictive accuracy compared with the use of tPSA alone for the whole sample and for the subgroup of men with low PSA (both p<0.0005).

Discussion

Because of their restricted expression patterns with high abundance in human prostate glands, PSA and hK2 have been thoroughly evaluated as candidate biomarkers for benign and malignant prostatic disease. The concentration of hK2 in prostate tissue, seminal plasma, and blood is only 1% of the concentration of PSA. However, it has been observed that the amount of hK2 transcripts is around 10-50% of the amount PSA transcripts (26), which might indicate that these closely related proteases may differ in regard to translation rates or protein stability.

The initial work on hK2 as a potential tumor marker was tissue studies from Darson and associates (8). They found more intense hK2-specific immunostaining in lymphatic metastases and in high-grade tumors compared with well-differentiated tumors and benign tissue, whereas contrary findings were reported for PSA. Herrala et al quantified expression by a conceptually different approach; in situ hybridization revealed that hK2 was expressed at higher levels in PCa tissue compared with benign prostate tissue (p<0.0005), whereas PSA expression had the reverse pattern (p=0.06) (9). The authors further reported that the hK2 gene (*KLK2*) but not the PSA gene (*KLK3*) was amplified in PCa tissue, which was suggested as one possible explanation for

relative changes in their protein expression. Lintula et al recently reported confirmatory findings using RT-PCR to quantify relative levels of hK2 and PSA mRNA in benign tissue and PCa. In their study, the ratio of hK2/PSA mRNA was significantly higher in cancer compared with benign tissue (p=0.03) and higher still in high-grade PCa (p=0.006) ([10]). This finding suggests that changes in relative expression levels of hK2 vs. PSA may be associated with carcinogenesis and progression, hence providing further evidence that hK2 might be a useful biomarker for PCa and, in particular, advanced disease.

How do these observations from tissue studies translate into protease concentrations in the circulation? The tight compartmentalization of PSA and hK2 in the normal prostate is altered in prostatic disease. The disintegration of the continuous layer of basal cells, a characteristic early feature of carcinogenesis, results in loss of the normal glandular architecture and allows substantial leakage of various proteins into circulation. The covariance of hK2 and PSA concentrations in blood has been determined to be generally <60%, suggesting that hK2 might have utility as an independent biomarker for PCa ([27]).

Several retrospective studies have investigated pre-treatment serum hK2 in patients who have subsequently undergone RP for clinically localized PCa. Increasing hK2 was significantly associated with cancer volume, presence of ECE, and high-grade PCa ([12-14]).

Our present study was intended to evaluate which marker in blood best predicts high-risk disease and BCR; patients with BCR are likely to eventually develop metastasis. We therefore studied a reasonably representative cohort of 867 men from a contemporary population treated with RP for clinically localized PCa at a single institution. We further elected to include fPSA and a recently published method for fhK2 detection into the analysis ([23]). Previous studies indicated that a low ratio of free to total PSA (%fPSA) is linked to advanced prostate pathology.

Others, however, were not able to confirm these findings. The ratio of free to total hK2 (%fhK2) has been measured in a set of 103 patients with prostate cancer, in whom it ranged from 17% to 131% (mean 81%) ([23]). However, no study has ever evaluated the clinical relevance of serum fhK2.

Our data demonstrate that serum tPSA levels significantly indicate the presence of ECE and SVI and risk of BCR in a heterogeneous population, in which tPSA ranges widely (here from 0.11 to 83 ng/ml). However, in the sub-group of patients with tPSA ≤ 10 ng/ml, tPSA revealed limited ability to reflect ECE, SVI, and BCR (AUC of 0.584, 0.542, and 0.566, respectively). Hence our data support recent findings from other investigators, who concluded that tPSA is not a predictor of treatment outcome in men with tPSA < 10 ng/ml, the group most commonly seen in clinical practice ([4-6]). Intriguingly, hK2 retained significant ability to mirror ECE, SVI, and BCR in the truncated PSA range (AUC of 0.625, 0.662, and 0.758, respectively).

The clinical relevance of our findings becomes significant in consideration of the high proportion of men with serum PSA ≤ 10 ng/ml in contemporary RP series. Particularly in the US, PSA levels at diagnosis have fallen dramatically because of widespread use of tPSA testing for the detection of PCa ([5]). As an example of a European population, among patients who recently underwent RP (from 2002 to 2003) at University Hospital Hamburg-Eppendorf, the percentage with tPSA ≤ 10 ng/ml increased to 82%. This trend indicates that the use of PSA testing may also significantly decrease the proportion of men with tPSA > 10 ng/ml at diagnosis in countries in which PSA screening is not officially recommended.

Results from our multivariable analysis demonstrate that a combination of several markers adds to the predictive ability of a single analyte. More accurate predictions of ECE, SVI, and BCR can be obtained by combining tPSA, fPSA, and hK2 in a multivariable model. This

observation may be related to a specific interaction of the various protease cascades, which presumably indicates pathological alteration of the prostate gland prior to clinical signs. Thus, biological variables should probably not be considered in isolation; more information can be derived from markers in combination. Markers that may be useful for analysis of prostate cancer include the prostate-specific tissue kallikreins or other markers of local cancer progression such as TGF-β_1, interleukin-6 receptor (28), or the urokinase-like plasminogen activation cascade (29, 30).

The ratio of fhK2 to thK2 in our study slightly decreased from a median of 88% in organ-confined tumors to 78% in cancers with SVI. In univariate analysis, both fhK2 and %fhK2 were associated with ECE, SVI, and BCR. Thus, hK2 in blood is not consistently in the free, unbound form in PCa patients. Significant proportions (median 15-20%) are inferred to be stably complexed with serpin-type antiproteases, and these proportions may vary in benign and in malignant prostate disease is the major source of hK2-elevation in blood. The diagnostic benefit of selective fhK2 determination, however, remains limited: according to our multivariable analysis, addition of fhK2 or %fhK2 provided no substantial increase in predictive accuracy for ECE, SVI, or BCR (data not shown). Further evaluations are warranted, including the application of fhK2 for discriminating cancer from non-cancer prior to prostate biopsy.

Several limitations may influence the validity of our findings. The retrospective study design (analysis of frozen serum) may have influenced accuracy of measurements of the analytes. However, the accuracy of the methods used in this study have been demonstrated for tPSA and fPSA measured in archived serum (31). This study used patients from a single institution with large surgical volume, and it featured unusually stringent pre-analytical workup

and assays of biomarkers; therefore, the findings may not be representative of all clinical settings.

In conclusion, these data support findings from various tissue studies and demonstrate that hK2 levels in serum independently indicate PCa of unfavorable prognosis. Serum hK2 testing might play a crucial role in clinical assessment of the risk of cancer progression following local therapy in PCa patients with only moderately elevated PSA, which is typical of the contemporary patient population. In future research, we plan to incorporate hK2 measurements into currently available risk models for clinically localized PCa to refine their predictive accuracy in the low PSA range. If possible, a biochemical serum profile of high-risk PCa should be developed from the combination of established and emerging markers of local progression.

Acknowledgements

References

1.   D'Amico AV, Whittington R, Malkowicz SB, Fondurulia J, Chen MH, Kaplan I, et al. Pretreatment nomogram for prostate-specific antigen recurrence after radical prostatectomy or external-beam radiation therapy for clinically localized prostate cancer. J Clin Oncol 1999;17:168–72.

2.   Kattan MW, Eastham JA, Stapleton AM, Wheeler TM, Scardino PT. A preoperative nomogram for disease recurrence following radical prostatectomy for prostate cancer. J Natl Cancer Inst 1998;90:766–71.

3.   Partin AW, Kattan MW, Subong EN, Walsh PC, Wojno KJ, Oesterling JE, et al. Combination of prostate-specific antigen, clinical stage, and Gleason score to predict pathological stage of localized prostate cancer. A multi-institutional update. JAMA 1997;277:1445–51.

4.   Stamey TA, Johnstone IM, McNeal JE, Lu AY, Yemoto CM. Preoperative serum prostate specific antigen levels between 2 and 22 ng./ml. correlate poorly with post-radical prostatectomy cancer morphology: prostate specific antigen cure rates appear constant between 2 and 9 ng./ml. J Urol 2002;167:103–11.

5.   Stamey TA, Caldwell M, McNeal JE, Nolley R, Hemenez M, Downs J. The prostate specific antigen era in the United States is over for prostate cancer: what happened in the last 20 years? J Urol 2004;172:1297–301.

6.   Freedland SJ, Aronson WJ, Kane CJ, Terris MK, Presti JC Jr, Trock B, Amling CL. Biochemical outcome after radical prostatectomy among men with normal preoperative serum prostate-specific antigen levels. Cancer 2004;101:748–53.

7.   Rittenhouse HG, Finlay JA, Mikolajczyk SD, Partin AW. Human Kallikrein 2 (hK2) and prostate-specific antigen (PSA): two closely related, but distinct, kallikreins in the prostate. Crit Rev Clin Lab Sci 1998;35:275–368.

8.   Darson MF, Pacelli A, Roche P, Rittenhouse HG, Wolfert RL, Saeid MS, et al. Human glandular kallikrein 2 expression in prostate adenocarcinoma and lymph node metastases. Urology 1999;53:939–44.

9.   Herrala AM, Porvari KS, Kyllonen AP, Vihko PT. Comparison of human prostate specific glandular kallikrein 2 and prostate specific antigen gene expression in prostate with gene amplification and overexpression of prostate specific glandular kallikrein 2 in tumor tissue. Cancer 2001;92:2975–84.

10.   Lintula S, Stenman J, Bjartell A, Nordling S, Stenman UH. Relative concentrations of hK2/PSA mRNA in benign and malignant prostatic tissue. Prostate 2005;63:324–9.

11.   Lilja H, Abrahamsson PA. Three predominant proteins secreted by the human prostate gland. Prostate 1988;12:29–38.

12.   Haese A, Graefen M, Becker C, Noldus J, Katz J, Cagiannos I, et al. The role of human glandular kallikrein 2 for prediction of pathologically organ confined prostate cancer. Prostate 2003;54:181–6.

13.   Steuber T, Niemela P, Haese A, Pettersson K, Erbersdobler A, Felix Chun KH, et al. Association of free-prostate specific antigen subfractions and human glandular kallikrein 2 with volume of benign and malignant prostatic tissue. Prostate 2005;63:13–18.

14.   Steuber T, Vickers AJ, Haese A, Becker C, Petterson K, Chun FK, et al. Risk assessment for biochemical recurrence prior to radical prostatectomy: significant enhancement

contributed by human glandular kallikrein 2 (hK2) and free prostate specific antigen (PSA) in men with moderate PSA-elevation in serum. Int J Cancer 2006;118:1234–40.

15. D'Amico AV, Whittington R, Malkowicz SB, Schultz D, Schnall M, Tomaszewski JE, Wein A. A multivariate analysis of clinical and pathological factors that predict for prostate specific antigen failure after radical prostatectomy for prostate cancer. J Urol 1995;154:131–8.

16. Epstein JI, Partin AW, Potter SR, Walsh PC. Adenocarcinoma of the prostate invading the seminal vesicle: prognostic stratification based on pathologic parameters. Urology 2000;56:283–8.

17. Hull GW, Rabbani F, Abbas F, Wheeler TM, Kattan MW, Scardino PT. Cancer control with radical prostatectomy alone in 1,000 consecutive patients. J Urol 2002;167:528–34.

18. Pound CR, Partin AW, Eisenberger MA, Chan DW, Pearson JD, Walsh PC. Natural history of progression after PSA elevation following radical prostatectomy. JAMA 1999;281:1591–7.

19. McNeal JE, Redwine EA, Freiha FS, Stamey TA. Zonal distribution of prostatic adenocarcinoma. Correlation with histologic pattern and direction of spread. Am J Surg Pathol 1988;12:897–906.

20. American Joint Committee on Cancer. AJCC Cancer Staging Manual. Philadelphia: Lippincott-Raven Publishers, 1997.

21. Amling CL, Bergstralh EJ, Blute ML, Slezak JM, Zincke H. Defining prostate specific antigen progression after radical prostatectomy: what is the most appropriate cut point? J Urol 2001;165:1146–51.

22. Mitrunen K, Pettersson K, Piironen T, Bjork T, Lilja H, Lovgren T. Dual-label one-step immunoassay for simultaneous measurement of free and total prostate-specific antigen concentrations and ratios in serum. Clin Chem 1995;41:1115–20.

23. Vaisanen V, Eriksson S, Ivaska KK, Lilja H, Nurmi M, Pettersson K. Development of sensitive immunoassays for free and total human glandular kallikrein 2. Clin Chem 2004;50:1607–17.

24. Harrell FEJ. Regression Modelling Strategies with Applications to Linear Models, Logistic Regression, and Survival Analysis. In. New York: Springer, 2001.

25. Noldus J, Graefen M, Haese A, Henke RP, Hammerer P, Huland H. Stage migration in clinically localized prostate cancer. Eur Urol 2000;38:74–8.

26. Ylikoski A, Karp M, Pettersson K, Lilja H, Lovgren T. Simultaneous quantification of human glandular kallikrein 2 and prostate-specific antigen mRNAs in peripheral blood from prostate cancer patients. J Mol Diagn 2001;3:111–22.

27. Becker C, Piironen T, Kiviniemi J, Lilja H, Pettersson K. Sensitive and specific immunodetection of human glandular kallikrein 2 in serum. Clin Chem 2000;46:198–206.

28. Shariat SF, Kattan MW, Traxel E, Andrews B, Zhu K, Wheeler TM, Slawin KM. Association of pre- and postoperative plasma levels of transforming growth factor beta(1) and interleukin 6 and its soluble receptor with prostate cancer progression. Clin Cancer Res 2004;10:1992–9.

29. Piironen T, Haese A, Huland H, et al. Enhanced discrimination of benign from malignant prostatic disease by novel selective measurements of cleaved forms of urokinase receptor in serum. Clin Chem 2006 [in press].

30.   Piironen T, Laursen B, Pass J, et al. Specific immunoassays for detection of intact and cleaved forms of the urokinase receptor. Clin Chem 2004;50:2059–68.

31.   Ulmert D, Becker C, Nilsson JA, Piironen T, Bjork T, Hugosson J, et al. Reproducibility and accuracy of measurements of free and total prostate-specific antigen in serum vs plasma after long-term storage at -20 degrees C. Clin Chem 2006;52:235–9.

Table 1: Clinical and pathologic characteristics of 867 patients treated with radical prostatectomy between 1997 and 2004. Values are frequency (percentage) or median (interquartile range).

Age	63	(59, 66)
Pretreatment PSA		
≤ 10.0 ng/ml	627	74
10.1-20 ng/ml	188	21
> 20 ng/ml	49	6
Clinical stage*		
T1c	616	71
T2a/b/c	234	27
T3	17	2
Biopsy Gleason score		
≤ 3+3	603	70
3+4 / 4+3	242	28
≥ 4+4	22	3
Pathologic stage*		
pT2a/b/c	619	71
pT3a	162	19
pT3b	86	10
Pathology Gleason score		
≤ 3+3	432	50
3+4 / 4+3	425	49
≥ 4+4	10	1

* 2002 AJCC

Table 2: Pre-treatment biomarker measurements for the entire cohort and for subsets with adverse pathologic findings. Data are presented as median (interquartile range).

Biomarker	Overall cohort n=867	ECE Observed n=249	SVI Observed n=87
tPSA (ng/ml)	7.23 (4.86, 10.46)	8.74 (5.94, 13.8)	10.10 (6.13, 17.0)
fPSA (ng/ml)	0.89 (0.62, 1.32)	0.98 (0.70, 1.40)	1.00 (0.70, 1.46)
thK2 (ng/ml)	0.08 (0.05, 0.12)	0.11 (0.07, 0.16)	0.13 (0.08, 0.22)
%fPSA	0.12 (0.09, 0.18)	0.11 (0.08, 0.15)	0.10 (0.08, 0.14)
	n=577	n=159	n=54
fhK2 (ng/ml)	0.07 (0.05, 0.10)	0.08 (0.06, 0.12)	0.09 (0.06, 0.14)
%fhK2	0.86 (0.74, 0.99)	0.79 (0.69, 0.92)	0.78 (0.68, 0.97)

Table 3: Univariate and multivariable regression analysis to assess association of pre-treatment levels of biomarkers with ECE and SVI for the overall cohort of 867 patients. The predictive accuracy of each variable or combination of biomarkers is given as area under curve (AUC). Bootstrap-corrected AUC values for multivariable models are given in parentheses.

Biomarker	Coefficient	95% CI	P Value	AUC	P Value: AUC vs tPSA AUC
Extracapsular Extension: Univariate Analysis					
tPSA / SD	0.59	0.41, 0.77	<0.0005	0.654	Ref
fPSA / SD	0.17	0.03, 0.31	0.016	0.564	<0.0005
%fPSA / SD	-0.52	-0.70, -0.34	<0.0005	0.631	0.3
thk2 / SD	0.67	0.49, 0.85	<0.0005	0.662	0.6
fhK2 / SD (n=577)	0.54	0.34, 0.74	<0.0005	0.619	0.4
%fhK2 / SD (n=577)	-0.46	-0.76, -0.17	0.002	0.620	0.4
Seminal Vesicle Invasion: Univariate Analysis					
tPSA / SD	0.47	0.29, 0.64	<0.0005	0.663	Ref
fPSA / SD	0.24	0.07, 0.40	0.005	0.577	0.0004
%fPSA / SD	-0.55	-0.84, -0.26	<0.0005	0.633	0.3
thk2 / SD	0.61	0.43, 0.79	<0.0005	0.719	0.09
fhK2 / SD (n=577)	0.53	0.32, 0.75	<0.0005	0.652	0.6
%fhK2 / SD (n=577)	-0.53	-1.01, -0.06	0.03	0.600	0.6
Extracapsular Extension: Multivariable Analysis					
tPSA / SD	0.75	0.48, 1.01	<0.0005	0.714 (0.711)	0.001
fPSA / SD	-0.76	-1.07, -0.46	<0.0005		
thk2 / SD	0.69	0.46, 0.93	<0.0005		

Seminal Vesicle Invasion: Multivariable Analysis					
tPSA / SD	0.50	0.21, 0.79	0.001		
f PSA / SD	-0.60	-0.99, -0.21	0.003	0.762 (0.755)	0.0005
thk2 / SD	0.64	0.40, 0.88	<0.0005		

Table 4: Univariate and multivariable regression analysis to assess association of pre-treatment levels of biomarkers with extracapsular extension and seminal vesicle invasion for 627 patients with pre-treatment tPSA ≤ 10 ng/ml. The predictive accuracy of each variable or combination of variables is given as area under curve (AUC). Bootstrap-corrected AUC values for multivariable models are given in parentheses.

Biomarker	Coefficient	95% CI	P Value	AUC	P Value: AUC vs tPSA AUC
Extracapsular Extension: Univariate Analysis					
tPSA / SD	0.97	0.32, 1.62	0.004	0.584	Ref
fPSA / SD	-0.10	-0.48, 0.28	0.6	0.491	0.04
%fPSA / SD	-0.31	-0.52, -0.09	0.005	0.573	0.7
thk2 / SD	0.84	0.51, 1.17	<0.0005	0.625	0.19
fhK2 / SD (n=430)	0.51	0.22, 0.8	0.001	0.594	0.8
%fhK2 / SD (n=430)	-0.34	-0.67, -0.01	0.046	0.606	0.6
Seminal Vesicle Invasion: Univariate Analysis					
tPSA / SD	0.54	-0.52, 1.60	0.3	0.542	Ref
fPSA / SD	-0.33	-1.02, 0.35	0.3	0.521	0.8
%fPSA / SD	-0.30	-0.67, 0.06	0.10	0.572	0.5
thk2 / SD	0.97	0.57, 1.37	<0.0005	0.662	0.03
fhK2 / SD (n=430)	0.73	0.38, 1.09	<0.0005	0.651	0.14
%fhK2 / SD (n=430)	-0.61	-1.25, 0.04	0.07	0.605	0.5
Extracapsular Extension: Multivariable Analysis					
tPSA / SD	1.11	0.33, 1.88	0.005	0.658 (0.650)	0.01
fPSA / SD	-1.01	-1.56, -0.47	<0.0005		
thk2 / SD	1.03	0.63, 1.42	<0.0005		

Seminal Vesicle Invasion: Multivariable Analysis				
tPSA / SD	0.85	-0.41, 2.12	0.19	
fPSA / SD	-1.65	-2.70, -0.59	0.002	0.716 (0.705)	0.002
thk2 / SD	1.30	0.80, 1.81	<0.0005	

Table 5: Univariate and multivariable Cox regression analysis to assess association of pre-treatment levels of biomarkers with biochemical recurrence. The predictive accuracy of each variable or combination of biomarkers is given as concordance index (c-index). Bootstrap-corrected c-indices for multivariable models are shown in parentheses.

Biomarker	Coefficient	95% CI	P Value	c-index	P Value: c-index vs tPSA c-index
All Patients (n= 784): Univariate Analysis					
tPSA / SD	0.38	0.29, 0.47	<0.0005	0.696	Ref
fPSA / SD	0.23	0.13, 0.33	<0.0005	0.632	<0.0005
%fPSA / SD	-0.43	-0.65, -0.20	<0.0005	0.597	<0.0005
thk2 / SD	0.46	0.37, 0.55	<0.0005	0.721	0.7
fhK2 / SD (n=515, with BCR=61)	0.42	0.28, 0.55	<0.0005	0.690	0.4
%fhK2 / SD (n=515, with BCR=61)	-0.67	-1.12, -0.23	0.003	0.621	<0.0005
PSA ≤ 10 ng/ml (n= 556): Univariate Analysis					
tPSA / SD	0.95	-0.03, 1.92	0.057	0.566	Ref
fPSA / SD	-0.03	-0.57, 0.51	0.9	0.452	0.3
%fPSA / SD	-0.17	-0.49, 0.14	0.3	0.526	0.19
thk2 / SD	0.97	0.73, 1.20	<0.0005	0.739	<0.0005
fhK2 / SD (n=377, with BCR=27)	0.79	0.55, 1.02	<0.0005	0.758	<0.0005
%fhK2 / SD (n=377, with BCR=27)	-0.55	-1.21, 0.12	0.11	0.614	0.07
All Patients: Multivariable Analysis					

tPSA / SD	0.32	0.16, 0.49	<0.0005		
fPSA / SD	-0.26	-0.50, -0.02	0.03	0.763 (0.752)	<0.0005
thk2 / SD	0.38	0.24, 0.53	<0.0005		

PSA ≤ 10 ng/ml: Multivariable Analysis					
tPSA / SD	1.35	0.25, 2.44	0.02		
fPSA / SD	-1.07	-1.85, -0.28	0.01	0.746 (0.742)	<0.0005
thk2 / SD	1.11	0.85, 1.36	<0.0005		